Radial oscillations of encapsulated microbubbles in viscoelastic liquids

Damir B. Khismatullin and Ali Nadim

Radial oscillations of encapsulated microbubbles in viscoelastic liquids

Damir B. Khismatullin[a) and Ali Nadim[b)
Department of Aerospace and Mechanical Engineering, Boston University, 110 Cummington Street, Boston, Massachusetts 02215

The small-amplitude radial oscillations of a gas microbubble encapsulated by a viscoelastic solid shell and surrounded by a slightly compressible viscoelastic liquid are studied theoretically. The Kelvin–Voigt and 4-constant Oldroyd models are used to describe the viscoelastic properties of the shell and liquid, respectively. The equation for radial oscillation is derived using the method of matched asymptotic expansions. Based on this equation, we present the expressions for damping coefficients and scattering cross sections at the fundamental frequency and at twice that frequency. The numerical maximization of the amplitude-frequency response function shows that the resonance frequency for the encapsulated microbubble highly depends on viscous damping, and therefore, significantly differs from the undamped natural frequency. The effects of the shell and liquid parameters on the resonance frequency and scattering cross sections are analyzed. © *2002 American Institute of Physics.* [DOI: 10.1063/1.1503353]

I. INTRODUCTION

Despite the fact that microbubbles covered with a biocompatible surface-active layer have been the subject of intense experimental research and commercial development for use as contrast agents for medical ultrasound diagnostics,[1–3] a rigorous theoretical description for the pulsations of such encapsulated bubbles in blood flow is not available. Existing theoretical models are based upon various forms of the Rayleigh–Plesset (RP) equation for spherical bubble oscillations, and attempt to take into account, often on the basis of unjustified conjectures, the elasticity and viscosity of the surfactant layer which is treated as a viscoelastic solid shell.[4,5] In particular, in the de Jong model[4,6,7] encapsulation provides additional damping of bubble oscillations and makes the bubble more "rigid." In doing so, a shell friction is included in the damping coefficient and a shell elasticity term is added in the Rayleigh–Plesset (RP) equation. Neither a normal stress balance at the bubble surface nor a rheological equation for the shell is considered. The heart of the Church model[5,8] is the modified RP equation which is derived from conservation of radial momentum assuming the existence of two interfaces: One between the gas and the shell and another between the shell and the surrounding liquid, i.e., taking into account the finite thickness of the encapsulating layer. The shell itself is modeled as a viscoelastic solid.

The standard RP equation holds only if the liquid surrounding a gas bubble is Newtonian and incompressible. These assumptions may be reasonable in certain inorganic aqueous media but not for living matter and, in particular, human tissue and blood.[9–12] Nonetheless, the RP-based mod-els are claimed to be "validated by extensive experimental results" by fitting the models, i.e., the *a priori* unknown values of shell elasticity and viscosity, to experimental measurements. In our view, such models cannot be accurately used to interpret *in vivo* measurements and our goal in the paper is to provide a more accurate description which can actually be used with confidence for this purpose. To date, no theoretical studies on radial oscillations of encapsulated microbubbles in compressible viscoelastic liquids are available. The effects of acoustic radiation are considered by Chin and Burns.[13] However, their model is simply a modified Trilling equation which is appropriate only for the pulsation of free microbubbles (without encapsulation) in Newtonian liquids.

A microbubble in a liquid undergoes forced radial oscillations when the ultrasound wave, the wavelength of which is much larger than the bubble radius, impinges upon it. The size of the bubble decreases in the positive half cycle of the ultrasound wave and increases in the negative one. The pulsating microbubble emits secondary ultrasound waves in the surrounding liquid (blood), i.e., it behaves as a source of sound. The microbubble, therefore, enhances the backscatter signal from blood and provides bright blood pool contrast, especially if it is driven at its resonance frequency. The most effective scatterer of ultrasound is a free microbubble: Its resonant scattering cross sections are of the order of a thousand times greater than its geometrical cross section.[14] However, such a microbubble dissolves very quickly after intravenous injection before entering the systemic circulation. Encapsulation extends the lifetime of the microbubble but degrades its scattering properties.[6] Also, the natural frequency of microbubble oscillations is augmented[5,15] by the elasticity of the encapsulating layer. The response of the surrounding tissue suppresses the backscattered signal of the microbubble at the fundamental (driving) frequency. Fortunately, a pulsating gas bubble is a highly nonlinear system. At rather large values of the acoustic pressure amplitude, it

a)Author to whom correspondence should be addressed. Present address: Department of Mathematics, Virginia Tech, VA 24061-0123.
b)Present address: Department of Mathematics, Claremont Graduate University, Claremont, CA 91711 and Keck Graduate Institute, Claremont, CA 91711.

generates a wide spectrum of harmonics and subharmonics.[16,17] When the bubble oscillations are resonant, the backscattered signal has harmonic and subharmonic components with decreasing intensity but strong enough to be used for diagnostic purposes. This has made possible the method of "second-harmonic imaging:" Ultrasound is transmitted at the fundamental frequency and received at twice that frequency.[18] Of vital importance for contrast harmonic imaging is, therefore, to know the correct expressions for the resonance frequency and the scattering cross sections at the driving frequency and at twice the driving frequency. These expressions are given and analyzed in the present paper.

There are other, more impressive areas of microbubble applications. The encapsulated bubbles with an average size less than that of a red blood cell ($\leqslant 10$ μm in size) are capable of penetrating even into the smallest capillaries and releasing drugs and genes, incorporated either inside them or on their surface, under the action of ultrasound.[19,20] These microbubbles can transport a specific drug to a specific site within the body (for instance, an anticancer drug to a specific tumor). The tissue-specific drug delivery will be more effective if targeting ligands are attached to the microbubble surface. The ligands (biotin or antibody) bind to the receptors (avidin or antigen) situated at the blood vessel walls of the target site and force the microbubble to attach to the blood vessel walls.[21] The attachment of microbubbles to the walls can assure targeted drug delivery. Under exposure to sufficiently high-amplitude ultrasound, these microbubbles would rupture, spewing drugs or genes, which are contained in their encapsulating layer, to the target tissue. Commercial development of these ideas is in its initial phase, but methods for preparing such microbubbles have already been patented.[22] The ultrasound-induced breakup has been observed for several ultrasound contrast agents, including albumin- and phospholipid-covered microbubbles.[23] An understanding of microbubble behavior is also important for a range of applications in biotechnology. The colloidal gas aphrons, which are microbubbles encapsulated by surfactant multilayers, are coming into use for the recovery of cells and proteins as well as for the enhancement of gas transfer in bioreactors.[24]

The remainder of the paper is structured as follows. Section II gives the governing equations for the radial flow of the viscoelastic liquid around an encapsulated microbubble. The 4-constant Oldroyd and Kelvin–Voigt constitutive equations are used to model the liquid and the shell, respectively. In Sec. III we construct the equation for radial oscillations of an encapsulated microbubble in a compressible viscoelastic liquid using the method of matched asymptotic expansions. The small-amplitude bubble oscillations are examined in Sec. IV. We derive the formulas for the first- and second-harmonic amplitudes of oscillation and present the expressions for the resonance frequency and the first- and second-harmonic scattering cross sections there. In Sec. V the damping coefficients for the encapsulated microbubble, the effects of damping on the resonance frequency as well as the dependencies of the resonance frequency and scattering cross sections on the shell and liquid parameters are analyzed. Section VI concludes the paper.
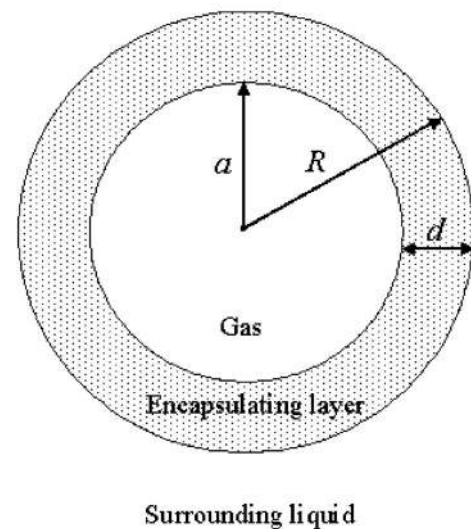

FIG. 1. Schematic sketch of an encapsulated bubble.

II. GOVERNING EQUATIONS

Consider spherically symmetric radial flow in an unbounded viscoelastic liquid which surrounds a gas bubble covered by an encapsulating layer. The layer is modeled as an incompressible viscoelastic solid shell and taken to be of finite thickness, i.e., we assume the existence of two interfaces: One between the gas and the encapsulating layer and the other between the layer and the surrounding liquid (Fig. 1). In writing the governing equations, we take into account the compressibility of the liquid but neglect the effects of gravity and other body forces; we also assume that the pressure is spatially uniform inside the bubble, the shell is incompressible, gas diffusion affects neither the velocity nor the stress fields, the temperature in the liquid remains constant during the oscillations, the gas within the bubble is polytropic, the partial pressure of the vapor is small compared with the gas pressure, and the bubble motion is purely radial, i.e., there is no rotation or shape deformation. Under these assumptions, the radial flow of the liquid around an encapsulated bubble is described in spherical coordinates (r, Θ, φ) by the equations of continuity

$$\frac{\partial \rho}{\partial t} + \frac{\partial (\rho v_r)}{\partial r} + \frac{2\rho v_r}{r} = 0, \tag{1}$$

and radial momentum

$$\rho\left(\frac{\partial v_r}{\partial t} + v_r \frac{\partial v_r}{\partial r}\right) = -\frac{\partial p}{\partial r} + (\mathbf{\nabla} \cdot \mathbf{\chi})_r, \tag{2}$$

the barotropic equation of state for the liquid

$$p_l = p_l(\rho_l), \tag{3}$$

a polytropic pressure-volume relationship for the gas

$$p_i = p_{i0}\left(\frac{a_0}{a}\right)^{3\kappa}, \tag{4}$$

the initial conditions

$$t=0: \quad a=a_0, \quad R=R_0, \quad v_r=0, \quad p_l=p_0, \quad \rho_l=\rho_{l0},$$
$$(5)$$

and the boundary conditions at the interfaces and infinity

$$r=a: \quad v_r=\frac{da}{dt}, \quad p_i=p_s-\chi_{rr}^{(s)}+\frac{2\sigma_1}{a}, \quad (6)$$

$$r=R: \quad v_r=\frac{dR}{dt}, \quad p_l-\chi_{rr}^{(l)}=p_s-\chi_{rr}^{(s)}-\frac{2\sigma_2}{R}, \quad (7)$$

$$r\to\infty: \quad v_r\to0, \quad p_l\to p_0. \quad (8)$$

Here t is time, r the radial coordinate, ρ the density, p the pressure, v_r the radial component of the velocity, χ the stress tensor, $a(t)$ the inner radius of the bubble, $R(t)$ the outer radius of the bubble (together with the encapsulating layer), p_i the internal pressure of the bubble (gas pressure), and κ a polytropic exponent. The subscript 0 refers to the unperturbed state of the bubble. The subscripts l and s identify liquid and shell parameters. Surface tension at the inner (gas-shell) and outer (shell-liquid) interfaces is denoted by σ_1 and σ_2, respectively. Equations (1) and (2) are integrated with respect to r from $a(t)$ to ∞ using the parameters appropriate for the shell ($\rho=\rho_{s0}$, $p=p_s$, $\chi=\chi^{(s)}$) and the liquid ($\rho=\rho_l$, $p=p_l$, $\chi=\chi^{(l)}$) in the regions (a,R) and (R,∞). Taking into account that $\chi_{\Theta\Theta}=\chi_{\varphi\varphi}$ for a purely radial flow and that the shell is incompressible, these equations can be rewritten in the form

$$\frac{\partial v_r}{\partial r}+\frac{2v_r}{r}=0, \quad \text{for } r\in(a,R),$$

$$\frac{\partial \rho_l}{\partial t}+\frac{\partial(\rho_l v_r)}{\partial r}+\frac{2\rho_l v_r}{r}=0, \quad \text{for } r\in(R,\infty),$$
$$(9)$$

$$\rho_{s0}\left(\frac{\partial v_r}{\partial t}+v_r\frac{\partial v_r}{\partial r}\right)=-\frac{\partial p_s}{\partial r}+\frac{\partial \chi_{rr}^{(s)}}{\partial r}+\frac{2}{r}[\chi_{rr}^{(s)}-\chi_{\Theta\Theta}^{(s)}],$$
$$\text{for } r\in(a,R),$$
$$(10)$$
$$\rho_l\left(\frac{\partial v_r}{\partial t}+v_r\frac{\partial v_r}{\partial r}\right)=-\frac{\partial p_l}{\partial r}+\frac{\partial \chi_{rr}^{(l)}}{\partial r}+\frac{2}{r}[\chi_{rr}^{(l)}-\chi_{\Theta\Theta}^{(l)}],$$
$$\text{for } r\in(R,\infty).$$

It is worth commenting on the validity of the above assumptions. Gas pressure may be considered uniform if the Mach number of the bubble wall motion, calculated with respect to the speed of sound in the gas, is much less than unity, and the wavelength of sound in the gas is much larger than the characteristic bubble radius.[25,26] Significant pressure nonuniformities would develop in a collapsing bubble and at frequencies that are large compared with the resonance frequency of free bubble oscillations.[26] The second condition for uniformity of the gas pressure implies that all pressure perturbations, leading to or generated by pulsations of the bubble, propagate in the gas, and hence in the liquid, as long waves. We can then consider a region of the liquid near the bubble surface, and thus the shell, to be incompressible.[27] Since gas diffusion in and out of the bubble manifests itself over time scales much longer than the period of bubble oscillations, we eliminate the gas transfer problem from con-

sideration. The constant temperature in the liquid may be explained by noting that the specific heat of the liquid is very large compared with that of the gas, i.e., "the liquid may be regarded as a thermostat that absorbs and gives off heat to the bubble walls without changing its temperature." [25] However, heat conduction through the bubble wall affects the bubble dynamics very strongly. Fortunately, the heat influx equation for the gas can be replaced by an approximate polytropic pressure-volume relationship in the case of a calorically perfect gas, uniform internal pressures, and small-amplitude bubble oscillations.[26,28,29] A polytropic exponent κ then takes the value from 1 (isothermal behavior) to γ_g (adiabatic behavior with γ_g being the ratio of constant-pressure to constant-volume specific heats for the gas) and the energy dissipation due to thermal effects is accounted for in the damping coefficient of radial oscillations[29,30] (effects of heat conduction on bubble oscillations are considered in Sec. V). In reality, the shell is not a solid material because the microbubble is encapsulated by a layer of surface-active molecules (lipids or proteins), which are mobile. This is the reason why we consider the nonzero (but small) surface tension at the outer interface. Given the small size of the bubble and hence the decreased mobility of surface-active molecules due to the small surface area of the interface, the assumption that the encapsulating layer is a *viscoelastic* solid is reasonable. Problems of shape deformation or rotation of the bubble are beyond the scope of the present paper. Finally, we neglect body forces and the partial pressure of the vapor for the sake of simplicity.

We employ the Kelvin–Voigt constitutive equation to model the shell,[31] i.e., we assume that

$$\chi^{(s)}=2(G_s\gamma+\mu_s\dot\gamma), \quad (11)$$

where

$$\gamma=\tfrac{1}{2}(\nabla\mathbf{u}+\nabla\mathbf{u}^\dagger) \quad \text{and} \quad \dot\gamma=\tfrac{1}{2}(\nabla\mathbf{v}+\nabla\mathbf{v}^\dagger) \quad (12)$$

are the strain and rate-of-strain tensors, $\mathbf{u}$ and $\mathbf{v}$ the displacement and velocity vectors, G_s and μ_s the shear modulus and the shear viscosity of the shell. It is common practice to employ the Kelvin–Voigt model for estimating the stresses in cell membranes.[32] The same model was used by Church[5] to account for viscous properties of elastic solid shells. Generally, the stress tensor in a linear viscoelastic solid has non-deviatoric terms proportional to tr(γ) and tr($\dot\gamma$), where "tr" denotes the trace of a tensor. However, these terms vanish due to the assumption of shell incompressibility. This is fully confirmed in the case of purely radial flow. Indeed, if we restrict our attention to purely radial pulsations of the microbubble, the strain and rate-of-strain tensors are only defined by the radial components of the displacement and velocity vectors. From Eq. (9) and boundary conditions (6) and (7) it follows that the radial velocity of shell particles is given by

$$v_r=\frac{a^2}{r^2}\frac{da}{dt}=\frac{R^2}{r^2}\frac{dR}{dt}. \quad (13)$$

It is easy to show that if the volume of the shell is constant during radial oscillations, the difference between the spheri-

cal volumes $V=4\pi(r+u_r)^3/3$ and $V_0=4\pi r^3/3$ associated with a shell particle (initially at position r) after and before radial deformation is equal to $C_1(t)=4\pi(a^3-a_e^3)/3$ or $C_2(t)=4\pi(R^3-R_e^3)/3$ [note $C_1(t)=C_2(t)$]. Here u_r is the radial displacement; r, a_e, R_e and $r+u_r$, a, R are, respectively, the unstrained and strained positions of the shell particle, the inner interface, and the outer interface. For infinitesimal displacements, i.e., when $u_r \ll a_0$ and hence $|a-a_e| \ll a_0$, we then have

$$u_r=\frac{a^2(a-a_e)}{r^2}=\frac{R^2(R-R_e)}{r^2}$$

and

$$\gamma_{rr}=-2\gamma_{\Theta\Theta}=-\frac{2a^2(a-a_e)}{r^3},$$

$$\dot{\gamma}_{rr}=-2\dot{\gamma}_{\Theta\Theta}=-\frac{2a^2}{r^3}\frac{da}{dt}. \tag{14}$$

Taking into account that $\gamma_{\Theta\Theta}=\gamma_{\varphi\varphi}$ and $\dot{\gamma}_{\Theta\Theta}=\dot{\gamma}_{\varphi\varphi}$ due to spherical symmetry, one may obtain from Eq. (12) that $\mathrm{tr}(\gamma)=\gamma_{rr}+\gamma_{\Theta\Theta}+\gamma_{\varphi\varphi}=0$ and $\mathrm{tr}(\dot{\gamma})=\dot{\gamma}_{rr}+\dot{\gamma}_{\Theta\Theta}+\dot{\gamma}_{\varphi\varphi}=0$. Finally, rr- and $\Theta\Theta$-components of the stress tensor take the forms

$$\chi_{rr}^{(s)}=-2\chi_{\Theta\Theta}^{(s)}=-\frac{4a^2}{r^3}\left[G_s(a-a_e)+\mu_s\frac{da}{dt}\right], \quad \text{for } r\in(a,R) \tag{15}$$

which agrees with formula (10) in Ref. 5. (Note once again that $\chi_{\Theta\Theta}=\chi_{\varphi\varphi}$ for pure radial flows.)

It should be noted that the unstrained inner radius of the bubble a_e is not ordinarily equal to the equilibrium radius a_0. This implies that there are nonzero stresses (or pre-stresses) in the shell even if the microbubble does not change its volume. The pre-stresses in the shell can be a result of gas diffusion. Suppose that a free microbubble of radius a_e is covered in a saturated liquid by a layer of surface-active material forming the shell layer. Initially, the stresses in the layer are zero. Then the microbubble begins to dissolve due to interfacial tension which creates an over-pressure in the gas inside the bubble relative to the pressure in the liquid. The contraction of the bubble leads to the straining of the shell, and hence to nonzero stresses inside the shell. The stresses, or more precisely the component of the stress tensor in the radial direction (radial stress), increase with decreasing bubble volume and act in opposition to interfacial tension. When the radius of microbubble reaches the value $a_0<a_e$, the radial stress in the layer is counterbalanced by interfacial tension and the microbubble stops shrinking. This counter-balance may be one of the reasons why encapsulated microbubbles are more stable than free ones.[5]

In a compressible liquid the stress tensor $\boldsymbol{\chi}^{(l)}$ consists of two parts. The first part is the shear stress tensor $\boldsymbol{\tau}^{(l)}$ that depends on the rate-of-strain tensor. If the liquid is Newtonian, this tensor looks as follows:[33]

$$\boldsymbol{\tau}^{(l)}=2\mu_l\left[\dot{\gamma}-\frac{\mathrm{tr}(\dot{\gamma})\mathbf{I}}{3}\right], \tag{16}$$

where μ_l is the shear viscosity of the liquid. The second part is the isotropic tensor $\boldsymbol{\nu}^{(l)}=f_0\mathbf{I}$ with f_0 being in general a function of invariants of the rate-of-strain tensor,[34] i.e., $f_0=f_0(I_1,I_2,I_3)$, where $I_1=\mathrm{tr}(\dot{\gamma})$, $I_2=\{[\mathrm{tr}(\dot{\gamma})]^2-\mathrm{tr}(\dot{\gamma}^2)\}/2$, and $I_3=\mathrm{Det}(\dot{\gamma})$. To a first approximation

$$\boldsymbol{\nu}^{(l)}=\kappa_v\mathrm{tr}(\dot{\gamma})\mathbf{I}, \tag{17}$$

κ_v is the second (or dilatational) viscosity of the liquid. Apart from the Newtonian and linear viscoelastic cases, the shear stress tensor has a finite trace,[35] i.e., $\mathrm{tr}[\boldsymbol{\tau}^{(l)}]\neq 0$. Therefore, if the liquid is compressible and/or the constitutive equation for the liquid is nonlinear, there is a "viscous" contribution to the mean pressure $p_m=-\mathrm{tr}[\boldsymbol{\pi}^{(l)}]/3$ [$\boldsymbol{\pi}^{(l)}=-p_l\mathbf{I}+\boldsymbol{\chi}^{(l)}$ is the total stress tensor in the liquid] that results in its variation from the thermodynamic pressure p_l in the liquid.

We assume that the liquid surrounding the encapsulated microbubble is viscoelastic or more specifically, the liquid obeys the 4-constant Oldroyd constitutive equation.[35] From (16) it follows that in the compressible case this equation should contain additional terms involving $\mathrm{tr}(\dot{\gamma})$:

$$\boldsymbol{\tau}^{(l)}+\lambda_1\frac{D_c}{Dt}\boldsymbol{\tau}^{(l)}+\lambda_3\left[\dot{\gamma}-\frac{1}{3}\mathrm{tr}(\dot{\gamma})\mathbf{I}\right]\mathrm{tr}[\boldsymbol{\tau}^{(l)}]$$

$$=2\mu_l\left\{\dot{\gamma}-\frac{1}{3}\mathrm{tr}(\dot{\gamma})\mathbf{I}+\lambda_2\frac{D_c}{Dt}\left[\dot{\gamma}-\frac{1}{3}\mathrm{tr}(\dot{\gamma})\mathbf{I}\right]\right\}. \tag{18}$$

Here λ_1, λ_2, and λ_3 are the material constants (the constants λ_1 and λ_2 are often referred to as relaxation and retardation times, respectively), D_c/Dt is the codeformational (contra-variant convected) time derivative

$$\frac{D_c\phi}{Dt}=\frac{D\phi}{Dt}-(\boldsymbol{\nabla}\mathbf{v})^\dagger\cdot\phi-\phi\cdot(\boldsymbol{\nabla}\mathbf{v}), \quad \phi=\tau \text{ or } \dot{\gamma}, \tag{19}$$

and $D/Dt=\partial/\partial t+\mathbf{v}\cdot\boldsymbol{\nabla}$ is the material time derivative. Straightforward analysis shows that if the liquid flow is purely radial, the first two diagonal components of the shear stress tensor are in the form

$$\left[1+\lambda_1\frac{D}{Dt}\right]\tau_{rr}^{(l)}-2\lambda_1\frac{\partial v_r}{\partial r}\tau_{rr}^{(l)}$$

$$=\frac{4\mu_l}{3}\left\{1-\frac{\lambda_3}{2}\mathrm{tr}[\boldsymbol{\tau}^{(l)}]-2\lambda_2\frac{\partial v_r}{\partial r}+\lambda_2\frac{D}{Dt}\right\}\left(\frac{\partial v_r}{\partial r}-\frac{v_r}{r}\right), \tag{20a}$$

$$\left[1+\lambda_1\frac{D}{Dt}\right]\tau_{\Theta\Theta}^{(l)}-2\lambda_1\frac{v_r}{r}\tau_{\Theta\Theta}^{(l)}$$

$$=-\frac{2\mu_l}{3}\left\{1-\frac{\lambda_3}{2}\mathrm{tr}[\boldsymbol{\tau}^{(l)}]-2\lambda_2\frac{v_r}{r}+\lambda_2\frac{D}{Dt}\right\}\left(\frac{\partial v_r}{\partial r}-\frac{v_r}{r}\right). \tag{20b}$$

Since $\mathrm{tr}[\boldsymbol{\tau}^{(l)}]=\tau_{rr}^{(l)}+2\tau_{\Theta\Theta}^{(l)}$ is not equal to zero, the shear stress tensor can be represented as the sum of deviatoric (traceless) and nondeviatoric tensors[36]

$$\boldsymbol{\tau}^{(l)}=\boldsymbol{\tau}^{(ld)}+\tfrac{1}{3}\mathrm{tr}[\boldsymbol{\tau}^{(l)}]\mathbf{I}. \tag{21}$$

Substituting (21) into Eqs. (20) and taking into account that

$$\tau_{\Theta\Theta}^{(ld)} = -\tfrac{1}{2}\tau_{rr}^{(ld)}, \tag{22}$$

one can obtain the system of two coupled differential equations for $\tau_{rr}^{(ld)}$ and $\mathrm{tr}[\boldsymbol{\tau}^{(l)}]$

$$\left[1 - \frac{4\lambda_1}{3}\left(\frac{\partial v_r}{\partial r} + \frac{v_r}{2r}\right) + \lambda_1 \frac{D}{Dt}\right]\tau_{rr}^{(ld)}$$

$$= -\frac{2}{3}\left(\lambda_3 - \frac{2\lambda_1}{3}\right)\left(\frac{\partial v_r}{\partial r} - \frac{v_r}{r}\right)\mathrm{tr}[\boldsymbol{\tau}^{(l)}]$$

$$+ \frac{4\mu_l}{3}\left[1 - \frac{4\lambda_2}{3}\left(\frac{\partial v_r}{\partial r} + \frac{v_r}{2r}\right) + \lambda_2\frac{D}{Dt}\right]\left(\frac{\partial v_r}{\partial r} - \frac{v_r}{r}\right), \tag{23a}$$

$$\left[1 - \frac{2\lambda_1}{3}\left(\frac{\partial v_r}{\partial r} + \frac{2v_r}{r}\right) + \lambda_1\frac{D}{Dt}\right]\mathrm{tr}[\boldsymbol{\tau}^{(l)}]$$

$$= 2\lambda_1\left(\frac{\partial v_r}{\partial r} - \frac{v_r}{r}\right)\tau_{rr}^{(ld)} - \frac{8\mu_l\lambda_2}{3}\left(\frac{\partial v_r}{\partial r} - \frac{v_r}{r}\right)^2. \tag{23b}$$

Such traceless stress tensor formulation for viscoelastic fluid flow is more suitable for analytical calculations. Also, as shown by Oliveira,[36] this formulation provides stability of numerical computations. Finally, the rr- and $\Theta\Theta$-components of the stress tensor for the radial flow of the 4-constant Oldroyd liquid around the encapsulated microbubble can be written as

$$\chi_{rr}^{(l)} = \tau_{rr}^{(ld)} + \frac{1}{3}\mathrm{tr}[\boldsymbol{\tau}^{(l)}] + \kappa_\nu\left(\frac{\partial v_r}{\partial r} + \frac{2v_r}{r}\right),$$

$$\chi_{\Theta\Theta}^{(l)} = -\frac{1}{2}\tau_{rr}^{(ld)} + \frac{1}{3}\mathrm{tr}[\boldsymbol{\tau}^{(l)}] + \kappa_\nu\left(\frac{\partial v_r}{\partial r} + \frac{2v_r}{r}\right), \tag{24}$$

where $r \in (R,\infty)$ and $\tau_{rr}^{(ld)}$ and $\mathrm{tr}[\boldsymbol{\tau}^{(l)}]$ are governed by Eqs. (23).

The reason we have adopted the 4-constant Oldroyd constitutive equation is to enable us to understand what would happen if the medium which surrounds the microbubble is not just viscous but also has some elastic properties. Even though blood by itself may show Newtonian behavior, as in large arteries, blood together with the surrounding tissue provide a medium which globally has both viscosity and elasticity. In that case, the simplest model that would capture these effects would be the linear Maxwell model, but it is not too much harder to include a retardation time and try to derive results which might have wider applicability (our results can be used for the interpretation of experimental data on small-amplitude oscillations of microbubbles in dilute polymer solutions). Finally, since we extend the analysis beyond just linearized theory, use of convective time derivatives makes sure that we do not miss any effects associated with the convective contribution to the time rates of change. We thus adopt the 4-constant Oldroyd model as a good first step in trying to account for both viscous and elastic effects in a general medium and still being able to make analytical progress. Further explanations are given in Sec. V.

Equations (3), (4), (9), (10), (15), (23), (24) and boundary conditions (6)–(8) comprise the full system of equations for the radial flow of a compressible viscoelastic liquid near the microbubble encapsulated by a viscoelastic solid shell.

We restrict our attention to the weakly compressible case for which the equation of state (3) contains only linear terms

$$\rho_l = \rho_{l0} + \frac{p_l - p_0}{C_l^2}, \quad C_l^2 = \left(\frac{dp_l}{d\rho_l}\right)_0, \tag{25}$$

(C_l is the speed of sound in the liquid). Then, substituting Eqs. (25) into Eqs. (24) and (9), defining the dimensionless variables

$$r_* = \frac{r}{a_0}, \quad t_* = \frac{Ut}{a_0}, \quad v_* = \frac{v_r}{U}, \quad a_* = \frac{a}{a_0}, \quad R_* = \frac{R}{a_0}, \tag{26a}$$

$$p_{\cdot*} = \frac{p_\cdot}{p_0}, \quad \chi_*^{(\cdot)} = \frac{\chi^{(\cdot)}}{p_0}, \quad \tau_*^{(l)} = \frac{\tau^{(l)}}{p_0}, \quad \rho_{l*} = \frac{\rho_l}{\rho_{l0}}, \tag{26b}$$

and denoting

$$M = \frac{U}{C_l}, \quad \mathrm{De} = \frac{U\lambda_1}{a_0}, \quad \lambda = \frac{\lambda_2}{\lambda_1}, \quad \eta = \frac{\lambda_3}{\lambda_1},$$

$$\mathrm{Re}_l = \frac{a_0\rho_{l0}U}{\mu_l}, \quad \mathrm{Re}_s = \frac{a_0\rho_{s0}U}{\mu_s}, \tag{27a}$$

$$G_s^* = \frac{G_s}{p_0}, \quad \kappa_\nu^* = \frac{U\kappa_\nu}{p_0a_0}, \quad \sigma_1^* = \frac{2\sigma_1}{p_0a_0}, \quad \sigma_2^* = \frac{2\sigma_2}{p_0a_0}, \tag{27b}$$

one can reduce the governing equations to the form:

$$r_* \in (a_*,R_*): \quad \frac{\partial v_*}{\partial r_*} + \frac{2v_*}{r_*} = 0, \tag{28a}$$

$$r_* \in (a_*,R_*): \quad \frac{\partial v_*}{\partial t_*} + v_*\frac{\partial v_*}{\partial r_*}$$

$$= \frac{\rho_{l0}}{\rho_{s0}}\left[-\frac{\partial p_{s*}}{\partial r_*} + \frac{\partial \chi_{*rr}^{(s)}}{\partial r_*} + \frac{3\chi_{*rr}^{(s)}}{r_*}\right], \tag{28b}$$

$$r_* \in (a_*,R_*): \quad \chi_{*rr}^{(s)} = -\frac{4a_*^2}{r_*^3}$$

$$\times \left[G_s^*\left(a_* - \frac{a_e}{a_0}\right) + \frac{\rho_{s0}}{\rho_{l0}\,\mathrm{Re}_s}\frac{da_*}{dt_*}\right], \tag{28c}$$

$$r_* \in (R_*,\infty): \quad M^2\left(\frac{\partial p_{l*}}{\partial t} + v_*\frac{\partial p_{l*}}{\partial r_*}\right)$$

$$+ [1 + M^2(p_{l*} - 1)]\frac{1}{r_*^2}\frac{\partial(r_*^2 v_*)}{\partial r_*} = 0, \tag{28d}$$

$$r_* \in (R_*,\infty): \quad [1 + M^2(p_{l*} - 1)]\left(\frac{\partial v_*}{\partial t_*} + v_*\frac{\partial v_*}{\partial r_*}\right)$$

$$= -\frac{\partial}{\partial r_*}\left\{p_{l*} - \frac{1}{3}\mathrm{tr}[\boldsymbol{\tau}_*^{(l)}]\right\}$$

$$+ \frac{\partial}{\partial r_*}\left[\frac{\kappa_\nu^*}{r_*^2}\frac{\partial(r_*^2 v_*)}{\partial r_*}\right] + \frac{\partial\tau_{*rr}^{(ld)}}{\partial r_*}$$

$$+ \frac{3\tau_{*rr}^{(ld)}}{r_*}, \tag{28e}$$

Phys. Fluids, Vol. 14, No. 10, October 2002

Radial oscillations of encapsulated microbubbles   3539

$$r_* \in (R_*, \infty): \quad \left[1 - \frac{4\mathrm{De}}{3}\left(\frac{\partial v_*}{\partial r_*} + \frac{v_*}{2r_*} \right) + \mathrm{De}\frac{D}{Dt_*} \right] \tau_{*rr}^{(ld)}$$

$$= -\frac{2\mathrm{De}}{3}\left(\eta - \frac{2}{3} \right)\left(\frac{\partial v_*}{\partial r_*} - \frac{v_*}{r_*} \right)\mathrm{tr}[\boldsymbol{\tau}_*^{(l)}]$$

$$+ \frac{4}{3\mathrm{Re}_l}\left[1 - \frac{4\lambda\mathrm{De}}{3}\left(\frac{\partial v_*}{\partial r_*} + \frac{v_*}{2r_*} \right) \right.$$

$$\left. + \lambda\mathrm{De}\frac{D}{Dt_*} \right]\left(\frac{\partial v_*}{\partial r_*} - \frac{v_*}{r_*} \right), \tag{28f}$$

$$r_* \in (R_*, \infty): \quad \left[1 - \frac{2\mathrm{De}}{3}\left(\frac{\partial v_*}{\partial r_*} + \frac{2v_*}{r_*} \right) + \mathrm{De}\frac{D}{Dt_*} \right]\mathrm{tr}[\boldsymbol{\tau}_*^{(l)}]$$

$$= 2\mathrm{De}\left(\frac{\partial v_*}{\partial r_*} - \frac{v_*}{r_*} \right)\tau_{*rr}^{(ld)} - \frac{8\lambda\mathrm{De}}{3\mathrm{Re}_l}$$

$$\times \left(\frac{\partial v_*}{\partial r_*} - \frac{v_*}{r_*} \right)^2, \tag{28g}$$

$$r_* = a_*: \quad v_* = \frac{da_*}{dt_*}, \quad p_{i*} = p_{s*} - \chi_{*rr}^{(s)} + \frac{\sigma_1^*}{a_*},$$

$$p_{i*} = \frac{p_{i0}a_*^{-3\kappa}}{p_0}, \tag{28h}$$

$$r_* = R_*: \quad v_* = \frac{dR_*}{dt},$$

$$p_{l*} - \tau_{*rr}^{(ld)} - \frac{1}{3}\mathrm{tr}[\boldsymbol{\tau}_*^{(l)}] - \frac{\kappa_\nu^*}{r_*^2}\frac{\partial(r_*^2 v_*)}{\partial r_*} \tag{28i}$$

$$= p_{s*} - \chi_{*rr}^{(s)} - \frac{\sigma_2^*}{R_*},$$

$$r_* \to \infty: \quad v_* \to 0, \quad p_{l*} \to 1. \tag{28j}$$

$$t_* = 0: \quad a_* = 1, \quad R_* = R_0/a_0, \quad v_* = 0, \quad p_{l*} = 1. \tag{28k}$$

Here M is the Mach number, De the Deborah number, Re_l and Re_s are the Reynolds numbers for the liquid and for the shell, respectively. The characteristic velocity $U = \sqrt{p_0/\rho_{l0}}$ is of the order of the bubble-wall velocity[25] and λ is the ratio of two (retardation and relaxation) time constants, which is greater than zero but smaller than unity for a viscoelastic liquid.[35] An asterisk denotes nondimensional quantities.

III. MATCHED ASYMPTOTIC EXPANSION

Because we consider small-amplitude oscillations of the microbubble covered by a thin shell ($R_* - a_* \ll a_*$) with the bubble-wall Mach number M much less than unity, the space between the outer bubble interface and infinity can be divided into three zones[27,37] (see Fig. 2):

(1) $r_* \in [R_{\mathrm{ex}}, \infty)$, $R_{\mathrm{ex}} \gg R_*$: The external zone (far from the bubble), where the liquid compressibility is significant but the nonlinear inertial forces produced by convective accelerations are negligibly small;

(2) $r_* \in [R_*, R_{\mathrm{in}}]$: The internal zone (near the bubble wall), where the liquid can be considered to be incompressible
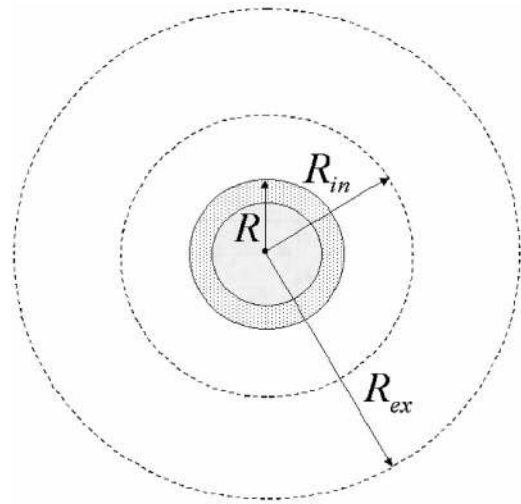

FIG. 2. Schematic of the internal and external zones.

and the radial motion is due to contraction and expansion of the bubble, but the nonlinear convective effects are significant;

(3) $r_* \in (R_{\mathrm{in}}, R_{\mathrm{ex}})$: An intermediate zone, where both the liquid compressibility and the nonlinear convective effects are fairly large.

In the first two zones one can construct asymptotic analytical solutions, the matching of which provides a solution in the third overlap zone. In what follows the indexes "ex" and "in" refer to the external and internal zones of the liquid.

A. Far from the bubble

Inasmuch as $r_* \gg 1$ in the far field, one can introduce a parameter $\varepsilon \ll 1$ such that

$$r_* = \frac{\tilde{r}_*}{\varepsilon}, \tag{29}$$

where $\tilde{r}_*$ is the radial coordinate that is $O(1)$ in the far field. This means that system (28) has two small parameters: M and ε. Let us assume $M \sim \varepsilon$ and

$$v_* = v_*^{(\mathrm{ex})} = \frac{\partial \varphi_{\mathrm{ex}}}{\partial r_*} = \varepsilon\frac{\partial \varphi_{\mathrm{ex}}}{\partial \tilde{r}_*}, \tag{30}$$

where φ_{ex} is the velocity potential in the external zone. We substitute (29) and (30) into Eqs. (28) and restrict our attention to the leading order terms. From Eqs. (28d) and (28e), we then have

$$M^2\frac{\partial p_{l*}^{(\mathrm{ex})}}{\partial t} + \frac{\varepsilon^2}{\tilde{r}_*^2}\frac{\partial}{\partial \tilde{r}_*}\left(\tilde{r}_*^2\frac{\partial \varphi_{\mathrm{ex}}}{\partial \tilde{r}_*} \right) = 0, \quad \frac{\partial^2 \varphi_{ex}}{\partial t_* \partial \tilde{r}_*} = -\frac{\partial p_{l*}^{(\mathrm{ex})}}{\partial \tilde{r}_*}. \tag{31}$$

Thus, nonlinear and viscous effects are negligibly small in the region far from the bubble and the motion of the liquid is wave-like because (31) is reduced to the following linear acoustic equations:

$$\frac{\partial^2 \varphi_{\mathrm{ex}}^*}{\partial t_*^2} = \frac{\varepsilon^2}{M^2\tilde{r}_*^2}\frac{\partial}{\partial \tilde{r}_*}\left(\tilde{r}_*^2\frac{\partial \varphi_{\mathrm{ex}}^*}{\partial \tilde{r}_*} \right) = \frac{1}{M^2 r_*^2}\frac{\partial}{\partial r_*}\left(r_*^2\frac{\partial \varphi_{\mathrm{ex}}^*}{\partial r_*} \right),$$

$$p_{l*}^{(\mathrm{ex})} = 1 - \frac{\partial \varphi_{\mathrm{ex}}^*}{\partial t_*}, \quad \varphi_{\mathrm{ex}} = \varphi_{\mathrm{ex}}^* + \int_0^{t_*} F(\tilde{t})d\tilde{t}$$

with the well-known solution

$$\varphi_{ex} = \frac{1}{r_*}[\psi_1(t_* - Mr_*) + \psi_2(t_* + Mr_*)] + \int_0^{t_*} F(\tilde{t})d\tilde{t}, \tag{32}$$

$$p_{l*}^{(ex)} = 1 - \frac{1}{r_*}[\psi_1'(t_* - Mr_*) + \psi_2'(t_* + Mr_*)], \tag{33}$$

where the prime denotes differentiation with respect to the argument, $F(\tilde{t})$ is an arbitrary function of time, and ψ_2 and ψ_1 characterize the acoustic waves which move towards and away from the bubble surface, respectively.

B. Near the bubble wall

Now $r_* \sim 1$ and the only small parameter in system (28) is M. Upon neglecting the terms of order M^2, Eq. (28d) takes the form

$$\frac{1}{r_*^2}\frac{\partial}{\partial r_*}\left(r_*^2 \frac{\partial \varphi_{in}}{\partial r_*}\right) = 0, \quad v_* = v_*^{(in)} = \frac{\partial \varphi_{in}}{\partial r_*}, \tag{34}$$

i.e., the standard incompressible formulation is valid near the outer bubble wall. As seen from Eq. (34) and boundary conditions (28h) and (28i), the radial velocity in the liquid near the bubble surface, like in the shell, obeys formula (13), whence it follows that

$$\varphi_{in} = \varphi_s = -\frac{R_*^2}{r_*}\frac{dR_*}{dt_*} = -\frac{a_*^2}{r_*}\frac{da_*}{dt_*}, \tag{35}$$

where φ_{in} and φ_s are the velocity potentials in the inner zone and the shell. In the incompressible case Eqs. (28f) and (28g) become

$$\left[1 - De\frac{\partial^2 \varphi_{in}}{\partial r_*^2} + De\frac{D}{Dt_*}\right]\tau_{*rr}^{(ld)}$$
$$= -De\left(\eta - \frac{2}{3}\right)\left(\frac{\partial^2 \varphi_{in}}{\partial r_*^2}\right)tr[\boldsymbol{\tau}_*^{(l)}]$$
$$+ \frac{2}{Re_l}\left[1 - \lambda De\frac{\partial^2 \varphi_{in}}{\partial r_*^2} + \lambda De\frac{D}{Dt_*}\right]\frac{\partial^2 \varphi_{in}}{\partial r_*^2}, \tag{36a}$$

$$\left[1 + De\frac{D}{Dt_*}\right]tr[\boldsymbol{\tau}_*^{(l)}] = 3De\left(\frac{\partial^2 \varphi_{in}}{\partial r_*^2}\right)\tau_{*rr}^{(ld)} - \frac{6\lambda De}{Re_l}\left(\frac{\partial^2 \varphi_{in}}{\partial r_*^2}\right)^2, \tag{36b}$$

and Eq. (28e) does not contain the dilatational viscosity term

$$\frac{\partial}{\partial r_*}\left\{\frac{\partial \varphi_{in}}{\partial t_*} + \frac{1}{2}\left(\frac{\partial \varphi_{in}}{\partial r_*}\right)^2 + p_{l*}^{(in)} - \tau_{*rr}^{(ld)} - \frac{1}{3}tr[\boldsymbol{\tau}_*^{(l)}]\right\} = \frac{3\tau_{*rr}^{(ld)}}{r_*}. \tag{37}$$

Here $p_{l*}^{(in)}$ is the liquid pressure in the internal zone. Obviously, one can put Eq. (28b) in the same form as (37)

$$\frac{\partial}{\partial r_*}\left\{\frac{\rho_{s0}}{\rho_{l0}}\left[\frac{\partial \varphi_s}{\partial t_*} + \frac{1}{2}\left(\frac{\partial \varphi_s}{\partial r_*}\right)^2\right] + p_{s*} - \chi_{*rr}^{(s)}\right\} = \frac{3\chi_{*rr}^{(s)}}{r_*}. \tag{38}$$

Upon integrating (37) from R_* to r_* and using (35), we obtain

$$p_{l*}^{(in)} - \tau_{*rr}^{(ld)} - \frac{1}{3}tr[\boldsymbol{\tau}_*^{(l)}]$$

$$= \left\{p_{l*}^{(in)} - \tau_{*rr}^{(l)} - \frac{1}{3}tr[\boldsymbol{\tau}_*^{(l)}]\right\}_{r_* = R_*}$$

$$+ \left[\frac{1}{r_*} - \frac{1}{R_*}\right]\frac{d}{dt_*}\left(a_*^2\frac{da_*}{dt_*}\right)$$

$$- \left[\frac{1}{r_*^4} - \frac{1}{R_*^4}\right]\frac{a_*^4}{2}\left(\frac{da_*}{dt_*}\right)^2 + 3\int_{R_*}^{r_*}\frac{\tau_{*\tilde{r}\tilde{r}}^{(ld)}}{\tilde{r}}d\tilde{r}. \tag{39}$$

Equation (39) provides $p_{l*}^{(in)}$ anywhere in the liquid near the bubble, upon invoking the equation of momentum for the shell and boundary conditions on the interfaces. Let us integrate (38) over r_* from a_* to R_* and substitute $[p_{s*} - \chi_{*rr}^{(s)}]_{r_* = a_*}$ from (28h) and $[p_{s*} - \chi_{*rr}^{(s)}]_{r_* = R_*}$ from (28i) into the resulting expression. We then have

$$\left\{p_{l*} - \tau_{*rr}^{(ld)} - \frac{1}{3}tr[\boldsymbol{\tau}_*^{(l)}]\right\}_{r_* = R_*}$$

$$= \frac{\rho_{s0}}{\rho_{l0}}\left\{\left[\frac{1}{R_*} - \frac{1}{a_*}\right]\frac{d}{dt_*}\left(a_*^2\frac{da_*}{dt_*}\right)\right.$$

$$\left. - \left[\frac{1}{R_*^4} - \frac{1}{a_*^4}\right]\frac{a_*^4}{2}\left(\frac{da_*}{dt_*}\right)^2\right\}$$

$$+ p_{i*} - \left(\frac{\sigma_1^*}{a_*} + \frac{\sigma_2^*}{R_*}\right) + 3\int_{a_*}^{R_*}\frac{\chi_{*\tilde{r}\tilde{r}}^{(s)}}{\tilde{r}}d\tilde{r}. \tag{40}$$

Equations (39) and (40) can be combined into the following formula for the pressure in the liquid in the near field of the bubble:

$$p_{l*}^{(in)} = p_{i*} - \left(\frac{\sigma_1^*}{a_*} + \frac{\sigma_2^*}{R_*}\right) - \frac{\rho_{s0}}{\rho_{l0}}\left\{\left(1 + \frac{\Delta_\rho a_*}{R_*}\right)a_*\frac{d^2 a_*}{dt_*^2}\right.$$

$$\left. + \left[\frac{3}{2} + \frac{\Delta_\rho a_*}{R_*}\left(2 - \frac{a_*^3}{2R_*^3}\right)\right]\left(\frac{da_*}{dt_*}\right)^2\right\} + \frac{a_*^2}{r_*}\frac{d^2 a_*}{dt_*^2}$$

$$- \left(\frac{a_*^4}{2r_*^4} - \frac{2a_*}{r_*}\right)\left(\frac{da_*}{dt_*}\right)^2 + \tau_{*rr}^{(ld)} + \frac{1}{3}tr[\boldsymbol{\tau}_*^{(l)}]$$

$$+ 3\left[\int_{a_*}^{R_*}\frac{\chi_{*\tilde{r}\tilde{r}}^{(s)}}{\tilde{r}}d\tilde{r} + \int_{R_*}^{r_*}\frac{\tau_{*\tilde{r}\tilde{r}}^{(ld)}}{\tilde{r}}d\tilde{r}\right], \tag{41}$$

where

$$\Delta_\rho = \frac{\rho_{l0} - \rho_{s0}}{\rho_{s0}}. \tag{42}$$

C. Equation for radial oscillation

Equations (35), (41) and (32), (33) represent asymptotic solutions of (28) in the region near the bubble surface and far from the bubble, respectively. To obtain an equation for radial oscillation of the encapsulated microbubble, one needs to match these solutions in the overlap zone $r_* \in [R_{in}, R_{ex}]$ on the assumption that this zone is at infinity ($r_* \to \infty$) with respect to the inner solution and near the bubble center r_*

→0) for the external solution. Matching conditions should be physically relevant and must not change if other features of flow, like the presence of vortices, had to be accounted for. This implies that matching of the velocity potentials, as was done by Prosperetti and Lezzi[37,38] for instance (see also Ref. 39), is not appropriate if the flow is not potential. Note that vortices appear in blood flow in large and curved vessels.[40,41] Due to acoustic streaming a rotational field may be produced in the vicinity of ultrasound contrast agents.[42] The physically correct matching conditions are the equality of volumetric flow rates $4\pi r_*^2 v_*$ and liquid pressures p_{l*}:[27]

$$4\pi r_*^2 v_*^{(in)}|_{r_*\to\infty} = 4\pi r_*^2 v_*^{(ex)}|_{r_*\to 0}, \tag{43a}$$

$$p_{l*}^{(in)}|_{r_*\to\infty} = p_{l*}^{(ex)}|_{r_*\to 0}. \tag{43b}$$

For the incompressible inner region, flow rate depends only on time

$$4\pi r_*^2 v_*^{(in)}|_{r_*\to\infty} = 4\pi r_*^2 \left.\frac{\partial\varphi_{in}}{\partial r_*}\right|_{r_*\to\infty} = 4\pi a_*^2 \frac{da_*}{dt_*}.$$

Therefore, upon using (30) and (32) condition (43a) can be rewritten in the form

$$a_*^2 \frac{da_*}{dt_*} = \{-\psi_1(t_*-Mr_*) - \psi_2(t_*+Mr_*)$$

$$+ Mr_*[-\psi_1'(t_*-Mr_*) + \psi_2'(t_*+Mr_*)]\}_{r_*\to 0}$$

$$= -\psi_1(t_*) - \psi_2(t_*),$$

whence it follows that

$$\psi_1(t_*) = -\psi_2(t_*) - Q(t_*), \quad Q(t_*) = a_*^2\frac{da_*}{dt_*}, \tag{44}$$

and the final asymptotic formulas for the velocity potential in the far and near fields are

$$\varphi_{ex} = \frac{1}{r_*}[\psi_2(t_*+Mr_*) - \psi_2(t_*-Mr_*)$$

$$- Q(t_*-Mr_*)] + \int_0^{t_*} F(\tilde{t})d\tilde{t},$$

$$\varphi_{in} = -\frac{Q(t_*)}{r_*}. \tag{45}$$

Using (33) and (45), we find the asymptotic solution for the liquid pressure in the far field

$$p_{l*}^{(ex)} = 1 - \frac{1}{r_*}[\psi_2'(t_*+Mr_*) - \psi_2'(t_*-Mr_*)$$

$$- Q'(t_*-Mr_*)]. \tag{46}$$

Taking into account that

$$\tau_{*rr}^{(l)}|_{r_*\to\infty} = 0,$$

substitution of Eqs. (41) and (46) into the matching condition (43b) leads to the following equation for radial oscillation of the encapsulated microbubble:

$$\frac{\rho_{s0}}{\rho_{l0}}\left\{\left(1+\frac{\Delta_\rho a_*}{R_*}\right)a_*\frac{d^2a_*}{dt_*^2} + \left[\frac{3}{2} + \frac{\Delta_\rho a_*}{R_*}\left(2 - \frac{a_*^3}{2R_*^3}\right)\right]\right.$$

$$\left.\times\left(\frac{da_*}{dt_*}\right)^2\right\} = p_{a*} - p_{\infty*}, \tag{47}$$

where

$$p_{a*} = p_{i*} - \left(\frac{\sigma_1^*}{a_*} + \frac{\sigma_2^*}{R_*}\right) + 3\left[\int_{a_*}^{R_*}\frac{\chi_{*\widetilde{rr}}^{(s)}}{\tilde{r}}d\tilde{r} + \int_{R_*}^{\infty}\frac{\tau_{*\widetilde{rr}}^{(ld)}}{\tilde{r}}d\tilde{r}\right], \tag{48}$$

$$p_{i*} = \frac{p_{i0}}{p_0}a_*^{-3\kappa},$$

$$p_{\infty*} = 1 - M\left(2\frac{d^2\psi_2}{dt_*^2} + \frac{d^2Q}{dt_*^2}\right). \tag{49}$$

We have thus obtained the generalized Rayleigh–Plesset (RP) equation for the radial motion of an encapsulated microbubble. In dimensional variables Eq. (47) is of the same form as derived by Church [see (5) in Ref. 5]. However, in the compressible formulation the p_∞ is not the liquid pressure at infinity but is related to the pressure in the matching zone, i.e., far from the bubble compared to its radius but near the bubble surface when compared with the wavelength and the distance between the bubble center and the transducer location. Note that the contribution of liquid viscoelasticity to the bubble oscillation is given by the following integral from R_* to infinity:

$$\int_{R_*}^{\infty}\frac{\tau_{*\widetilde{rr}}^{(ld)}}{\tilde{r}}d\tilde{r},$$

whence it follows that the compressibility corrections to Eq. (18), which are not small in the zone far from the bubble, should be taken into account.

For many decades theoretical analyses of bubble dynamics were based on the incompressible Rayleigh–Plesset equation, according to which the driving pressure was applied at an infinitely distant position. Nonetheless, there was good agreement between the solution of the RP equation and the experimental data only if the pressure measured by a hydrophone at the location of the bubble was used as the driving pressure in the RP equation. This has been somewhat of a paradox among experimentalists and theoreticians about the location and magnitude of the pressure that actually drives the motion of the bubble.[43] This paradox can be resolved only if a finite speed of sound and spherical convergence of acoustic waves in the liquid are accounted for. Any pressure disturbance generated in a liquid by a transducer at infinity never reaches the bubble. Even if the distance between the transducer and the bubble is finite, we should take into account an increase in the wave amplitude as the bubble surface is approached until the wave reaches the inner (incompressible) zone. Hence, the pressure at infinity should be replaced in the RP equation by the pressure that is measured at the outer edge of the inner zone, i.e., at the distance $r_* = R_{in}$ to ensure that this equation is in good agreement with

experimental results. Moss[44] has shown that the appropriate driving pressure is that within roughly 25 bubble radii from the bubble, i.e., $R_{in} \approx 25 R_*$.

From a theoretical point of view, the driving pressure $p_\infty(t) = p_0 p_{\infty*}$ is given by (49). In order to specify $\psi_2(t)$, and hence $p_{\infty*}$, we should consider the evolution of the pressure $p_R(t_*)$ at $r_* = R_t$ (R_t is the dimensionless distance between the transducer and the bubble center). Bubble oscillations are then described by the RP equation and the following difference equation for ψ_2 [derived from (46)] with both lagging and leading times:[27,45]

$$
p_R(t_*) = p_0 - \frac{p_0}{R_t} [\psi_2'(t_* + M R_t) \\
- \psi_2'(t_* - M R_t) - Q'(t_* - M R_t)].
$$ (50)

In this paper, we do not consider the boundary condition (50) and assume that the function $\psi_2(t_*)$ is sinusoidal

$$
\psi_2(t_*) = \Psi \sin \omega t_* = -\frac{\Psi}{2} [i \exp i \omega t_* + c.c.],
$$ (51)

where Ψ is a constant, ω is the nondimensional angular driving frequency, and c.c. means complex conjugate.

The term $d^2 Q(t_*)/dt_*^2$ in (49) involves the third-order derivative of the bubble radius a_*. This difficulty can be obviated in the small Mach number regime ($M \ll 1$).[37,45] It is apparent that

$$
\frac{1}{a_*} \frac{dQ}{dt_*} = \left(1 + \frac{\Delta_\rho a_*}{R_*}\right)^{-1} \left\{ \left(1 + \frac{\Delta_\rho a_*}{R_*}\right) a_* \frac{d^2 a_*}{dt_*^2} \right.\\
+ \left[\frac{3}{2} + \frac{\Delta_\rho a_*}{R_*}\left(2 - \frac{a_*^3}{2 R_*^3}\right)\right] \left(\frac{da_*}{dt_*}\right)^2 \\
\left. + \frac{1}{2}\left(1 + \frac{\Delta_\rho a_*^4}{R_*^4}\right) \left(\frac{da_*}{dt_*}\right)^2 \right\}.
$$ (52)

The first two terms on the right-hand side of (52) can be replaced by the right-hand side of Eq. (47). In view of the fact that if the Mach number is small, the following rough estimate is valid:[45]

$$
\left(M \frac{d^2 Q}{dt_*^2}\right) \bigg/ \left(a_* \frac{d^2 a_*}{dt_*^2}\right) \sim M \frac{da_*}{dt_*} \sim \varepsilon_a \ll 1,
$$

substitution of (47) into (52) and subsequent differentiation yields

$$
M \frac{d^2 Q}{dt_*^2} = M \frac{d}{dt}[a_* F_0(p_{a*} - p_{I*})] + \frac{\rho_{s0} M}{\rho_{l0}} \\
\times \left[\left(F_1 \frac{da_*}{dt_*}\right) a_* \frac{d^2 a_*}{dt_*^2} + \frac{1}{2}\frac{d}{dt}(a_* F_1)\right. \\
\left. \times \left(\frac{da_*}{dt_*}\right)^2\right] + O\left\{M^2 \frac{d}{dt}[a_* F_0 Q''(t_*)]\right\},
$$ (53)

where

$$
F_0(t_*) = \frac{\rho_{l0}}{\rho_{s0}}\left(1 + \frac{\Delta_\rho a_*}{R_*}\right)^{-1},
$$

$$
F_1(t_*) = F_0(t_*)\left(1 + \frac{\Delta_\rho a_*^4}{R_*^4}\right)
$$ (54)

and

$$
p_{I*} = 1 - 2M \frac{d^2 \psi_2}{dt_*^2}.
$$ (55)

The incident pressure p_{I*} is not equal to the driving pressure $p_{\infty*}$ but takes into account the convergent waves coming to the bubble from the transducer. It can be considered as the liquid pressure at the location of the bubble center in the absence of the bubble,[37] because (i) this pressure results from the external solution $p_{l*}^{(ex)}$ at $r_* \to 0$, (ii) there is no inner zone in the case of pure liquid. The correction term on the right-hand side of Eq. (53) is negligible compared to the terms which have been kept, provided that da_*/dt_* is itself small.[45]

To eliminate the variables $\chi_{*rr}^{(s)}$ and $\tau_{*rr}^{(ld)}$, we should calculate the integrals in (48). From (28c) it follows that the first integral can be evaluated as

$$
\int_{a_*}^{R_*} \frac{\chi_{*\widetilde{r}\widetilde{r}}^{(s)}}{\widetilde{r}} d\widetilde{r} = -\frac{4(R_0^3 - a_0^3)}{3 a_0^3 R_*^3} \\
\times \left[G_s^*\left(1 - \frac{a_e}{a_0 a_*}\right) + \frac{\rho_{s0}}{\rho_{l0} Re_s a_*}\frac{da_*}{dt_*}\right],
$$ (56)

where the unstrained equilibrium radius is

$$
a_e = a_0(1 + Z), \quad Z = \frac{1}{4 G_s^*}\left(\sigma_1^* + \frac{a_0 \sigma_2^*}{R_0}\right)\frac{R_0^3}{R_0^3 - a_0^3}.
$$ (57)

When deriving (56), we have taken into account that for an incompressible shell, the outer radius of the bubble, R_*, can be expressed in terms of the inner radius a_* as $R_* = \sqrt[3]{a_*^3 + (r_0/a_0)^3}$ with $r_0 = \sqrt[3]{R_0^3 - a_0^3}$ being a constant. The formula for a_e has been obtained from the conditions (28b), (28c), (28h), and (28i) at $t_* = 0$ under the assumption that $p_{i0} = p_0$ (the encapsulated microbubbles are permeable to gas).[5]

The calculation of the second integral is more intricate because of the presence of the material derivative D/Dt_* and the trace of the shear stress tensor tr$[\tau_*^{(l)}]$ in (28f). However, in the case of small deviations of the bubble radius from the equilibrium value: $a_*(t_*) = 1 + x(t_*)$, $v_* \sim x(t_*)$, when the nondimensional perturbation $x(t_*) \ll 1$, from Eq. (28g) it follows that tr$[\tau_*^{(l)}]$ is of the order of $x^2(t_*)$. This means that in Eq. (28f) the term

$$
\frac{2De}{3}\left(\eta - \frac{2}{3}\right)\left(\frac{\partial v_*}{\partial r_*} - \frac{v_*}{r_*}\right) tr[\tau_*^{(l)}],
$$

is a cubic nonlinearity, which cannot affect the first and second harmonics of bubble oscillation (see details in the Appendix). Of course, in the case of large-amplitude bubble oscillations (bubble collapse, sonoluminescence, etc.), the trace of the shear stress tensor should be taken into account.[46] But because we consider the linear and quadratic

nonlinear effects only, we remove this term from the constitutive equation (28f). Note that it is exactly zero if $\lambda_3 = 2\lambda_1/3$. Then, Eq. (28f) can be simplified by using the Lagrangian coordinate $y = r_*^3 - a_*^3$ and taking into account that $v_* = Q(t_*)/r_*^2$ in the inner zone [see Eq. (36a)]:

$$\tau_{*rr}^{(l)} = -\frac{4}{\text{DeRe}_l[y + a_*^3(t_*)]^{2/3}} \int_0^{t_*} \exp\left(\frac{\tilde{t} - t_*}{\text{De}}\right)$$
$$\times \left\{ \frac{Q(\tilde{t}) + \lambda \text{De} Q'(\tilde{t})}{[y + a_*^3(\tilde{t})]^{1/3}} - \frac{\lambda \text{De} Q^2(\tilde{t})}{[y + a_*^3(\tilde{t})]^{4/3}} \right\} d\tilde{t}. \quad (58)$$

Substituting (58) into the second integral in (48) and integrating over y from $R_*^3(t_*) - a_*^3(t_*)$ to ∞ result in the formula

$$q(t_*) = 3\int_{R_*}^{\infty} \frac{\tau_{*rr}^{(ld)}}{\tilde{r}} d\tilde{r} = \frac{6}{\text{DeRe}_l} \int_0^{t_*} \exp\left(\frac{\tilde{t} - t_*}{\text{De}}\right) [H_1(\tilde{t}, t_*) + H_2(\tilde{t}, t_*)] d\tilde{t}, \quad (59a)$$

$$H_1(\tilde{t}, t_*) = \left\{ \frac{Q(\tilde{t}) + \lambda \text{De} Q'(\tilde{t})}{a_*^3(\tilde{t}) - a_*^3(t_*)} - \frac{\lambda \text{De} Q^2(\tilde{t})}{[a_*^3(\tilde{t}) - a_*^3(t_*)]^2} \right\}$$
$$\times \left\{ 1 - \left[1 + \frac{a_*^3(\tilde{t}) - a_*^3(t_*)}{R_*^3(\tilde{t})} \right]^{2/3} \right\}, \quad (59b)$$

$$H_2(\tilde{t}, t_*) = -\frac{2\lambda \text{De} Q^2(\tilde{t})}{R_*^3(\tilde{t})[a_*^3(\tilde{t}) - a_*^3(t_*)]^2}$$
$$\times \left\{ 1 - \left[1 + \frac{a_*^3(\tilde{t}) - a_*^3(t_*)}{R_*^3(\tilde{t})} \right]^{-1/3} \right\}. \quad (59c)$$

Note that the integrand in (59a) is not singular at $\tilde{t} = t_*$ if deviations of the bubble radius from the equilibrium value are small. Upon retaining linear and quadratic nonlinear terms, integral (59) takes the form

$$q(t_*) = -\frac{4a_0^3}{\text{Re}_l R_0^3} \left[\left(1 - \frac{5a_0^3}{2R_0^3} x \right) q_1(t_*) \right.$$
$$\left. + \left(2 - \frac{a_0^3}{2R_0^3} \right) q_2(t_*) \right], \quad (60a)$$

$$\left[1 + \text{De} \frac{d}{dt_*} \right] q_1(t_*) = \left[1 + \lambda \text{De} \frac{d}{dt_*} \right] \frac{dx}{dt_*},$$
$$\left[1 + \text{De} \frac{d}{dt_*} \right] q_2(t_*) = \left[1 + \lambda \text{De} \frac{d}{dt_*} \right] x \frac{dx}{dt_*}. \quad (60b)$$

An alternative derivation of (60) is given in the Appendix. If we make use of the linear Jeffreys constitutive equation, Eq. (60a) will look as follows:

$$q(t_*) = -\frac{4a_0^3}{\text{Re}_l R_0^3} \left[q_1(t_*) + \left(2 - \frac{3a_0^3}{R_0^3} \right) q_2(t_*) \right]. \quad (61)$$

The difference between Eq. (60a) and the latter equation is the quadratic nonlinear term

$$N = \frac{10a_0^6}{\text{Re}_l R_0^6} [x q_1(t_*) - q_2(t_*)], \quad (62)$$

which represents the contribution from convective terms of the constitutive equation to the second harmonic of bubble oscillation.

Finally, substituting expression (53) into Eq. (47), we obtain the equation

$$\frac{\rho_{s0}}{\rho_{l0}} \left\{ \left(1 + \frac{\Delta_\rho a_*}{R_*} - MF_1 \frac{da_*}{dt_*} \right) a_* \frac{d^2 a_*}{dt_*^2} \right.$$
$$\left. + \left[\frac{3}{2} + \frac{\Delta_\rho a_*}{R_*} \left(2 - \frac{a_*^3}{2R_*^3} \right) - \frac{M}{2} \frac{d}{dt_*} (a_* F_1) \right] \left(\frac{da_*}{dt_*} \right)^2 \right\}$$
$$= p_{a*} - p_{I*} + M \frac{d}{dt_*} [a_* F_0 (p_{a*} - p_{I*})], \quad (63a)$$

$$p_{a*} = \frac{p_{i0}}{p_0} a_*^{-3\kappa} - \left(\frac{\sigma_1^*}{a_*} + \frac{\sigma_2^*}{R_*} \right) - \frac{4(R_0^3 - a_0^3)}{3a_0^3 R_*^3}$$
$$\times \left[G_s^* \left(1 - \frac{a_e}{a_0 a_*} \right) + \frac{\rho_{s0}}{\rho_{l0} \text{Re}_s a_*} \frac{da_*}{dt_*} \right] + q(t_*). \quad (63b)$$

Under the conditions $\rho_{s0} = \rho_{l0}$, when $\Delta_\rho = 0$ and $F_0 = F_1 = 1$, Eq. (63) simplifies to the equation for the oscillation of a free bubble

$$\left(1 - M \frac{da_*}{dt_*} \right) a_* \frac{d^2 a_*}{dt_*^2} + \frac{3}{2} \left(1 - \frac{M}{3} \frac{da_*}{dt_*} \right) \left(\frac{da_*}{dt_*} \right)^2$$
$$= \left(1 + M \frac{da_*}{dt_*} \right) (p_{a*} - p_{I*}) + M a_* \frac{d}{dt_*} (p_{a*} - p_{I*}).$$
$$\quad (64)$$

If the liquid is Newtonian and the shell thickness is zero, the dimensional version of Eq. (64) is of the same order as the Keller–Miksis equation[47] [see also (6.8) in Ref. 37].

IV. FIRST- AND SECOND-HARMONIC RESPONSE

A. Equations for perturbations

Let us consider small-amplitude oscillations of the encapsulated microbubble in the sinusoidal acoustic field (51), i.e., when the incident pressure

$$p_{I*} = 1 - P_A \sin \omega t_* = 1 + \frac{P_A}{2} [i \exp(i\omega t_*) + \text{c.c.}],$$
$$P_A = -2\omega^2 M \Psi. \quad (65)$$

The dimensionless amplitude of this field is small such that $P_A = \varepsilon_p P$, where $P \sim O(1)$ and $\varepsilon_p \ll 1$. The solution of Eq. (63) can then be expanded in powers of the parameter ε_p

$$a_* = 1 + x, \quad R_* = \frac{R_0}{a_0} \left[1 + \frac{a_0^3}{R_0^3} x + \frac{a_0^3}{R_0^3} \left(1 - \frac{a_0^3}{R_0^3} \right) x^2 + O(x^3) \right], \quad (66a)$$

$$x = x(t_*; \varepsilon_p) = \varepsilon_p x_1(t_*) + \varepsilon_p^2 x_2(t_*) + \cdots, \quad (66b)$$

which are then inserted into (60) and (63). At orders ε_p and ε_p^2 we then obtain the equations for the first- and second-

order perturbations in the inner radius of the microbubble, $x_1(t_*)$ and $x_2(t_*)$, respectively. Under the assumption that $q_1(t_*) = \varepsilon_p q_1^{(1)}(t_*) + \varepsilon_p^2 q_1^{(2)}(t_*) + o(\varepsilon_p^2)$ and $p_{i0} = p_0$, the first-order equations look as follows:

$$\alpha_0 \frac{d^2 x_1}{dt_*^2} + \delta_0 \frac{dx_1}{dt_*} + \gamma_0 x_1 + \frac{4a_0^3}{\mathrm{Re}_l R_0^3}\left[1 + \Lambda \frac{d}{dt_*}\right] q_1^{(1)}(t_*)$$

$$= -\frac{P(i - \Lambda\omega)}{2}\exp i\omega t_* + \text{c.c.}, \tag{67a}$$

$$\left[1 + \mathrm{De}\frac{d}{dt_*}\right] q_1^{(1)}(t_*) = \left[1 + \lambda\mathrm{De}\frac{d}{dt_*}\right]\frac{dx_1}{dt_*}. \tag{67b}$$

Here

$$\Lambda = \frac{\rho_{l0} M}{\rho_{s0}}\left(1 + \frac{\Delta_\rho a_0}{R_0}\right)^{-1}, \tag{68a}$$

$$\alpha_0 = \frac{\rho_{s0}}{\rho_{l0}}\left[1 + \frac{\Delta_\rho a_0}{R_0} + \frac{4\Lambda}{\mathrm{Re}_s}\left(1 - \frac{a_0^3}{R_0^3}\right)\right], \tag{68b}$$

$$\gamma_0 = 3\kappa - \sigma_1^* - \frac{\sigma_2^* a_0^4}{R_0^4} + 4G_s^*\left(1 - \frac{a_0^3}{R_0^3}\right)\left[1 + \left(1 + \frac{3a_0^3}{R_0^3}\right)Z\right], \tag{68c}$$

$$\delta_0 = \frac{4\rho_{s0}}{\rho_{l0}\mathrm{Re}_s}\left(1 - \frac{a_0^3}{R_0^3}\right) + \Lambda\gamma_0, \tag{68d}$$

and Z is given by (57). Note that Eq. (67a) is simply a damped harmonic oscillator equation for $x_1(t_*)$ which is forced by the right-hand side and is coupled to $q_1^{(1)}(t_*)$, which in turn accounts for viscoelastic behavior of the exterior liquid through (67b). We seek the solution of (67) in the form

$$\begin{bmatrix} x_1(t_*) \\ q_1^{(1)}(t_*) \end{bmatrix} = \begin{bmatrix} x_{1f}(t_*) \\ q_{1f}(t_*) \end{bmatrix} + \frac{1}{2}\begin{bmatrix} A_1 \\ Q_1 \end{bmatrix}\exp(i\omega t_*) + \text{c.c.} \tag{69}$$

with the complex amplitudes A_1 and Q_1 that can be considered as functions of the dimensionless angular frequency ω. The solution (69) contains the homogeneous term, or the complementary function $[x_{1f}(t_*)\ q_{1f}(t_*)]^\top$. This term describes free oscillations of the bubble which are exponentially damped in time. We consider only forced oscillations and take the complementary function to be zero: $x_{1f}(t_*) = q_{1f}(t_*) = 0$. Equation (67b) is then reduced to an algebraic relationship between Q_1 and A_1

$$\frac{Q_1}{A_1} = \nu(\omega) = \frac{\mathrm{De}(1 - \lambda)\omega^2 + i\omega(1 + \lambda\mathrm{De}^2\omega^2)}{1 + \mathrm{De}^2\omega^2}. \tag{70}$$

Substitution of (69) into Eq. (67a) gives, in view of (70), the formula for the first-harmonic amplitude A_1 of bubble oscillations

$$\frac{A_1}{P} \equiv A_{1P}(\omega) = -i\frac{1 + i\Lambda\omega}{D(\omega) + i\omega\delta(\omega)}, \tag{71}$$

where

$$D(\omega) = \gamma_0 - \left(\alpha_0 + \frac{4a_0^3\Lambda}{\mathrm{Re}_l R_0^3}\right)\omega^2$$

$$+ \frac{4a_0^3\mathrm{De}(1 - \lambda)(1 + \Lambda\mathrm{De}\omega^2)\omega^2}{\mathrm{Re}_l R_0^3(1 + \mathrm{De}^2\omega^2)}, \tag{72a}$$

$$\delta(\omega) = \delta_0 + \frac{4a_0^3}{\mathrm{Re}_l R_0^3}\left[1 - \frac{\mathrm{De}(1 - \lambda)(\mathrm{De} - \Lambda)\omega^2}{1 + \mathrm{De}^2\omega^2}\right]. \tag{72b}$$

As seen from (72), the smaller the difference between the relaxation and retardation times (larger λ), the smaller the liquid elasticity effects on bubble oscillations will be.

The nonlinear component $q_2(t_*)$ of the integral $q(t_*)$ which can be represented as $q_2(t_*) = \varepsilon_p^2 q_2^{(1)}(t_*) + o(\varepsilon_p^2)$, should be included in the second-order equations. From the second equation in (60b) and solution (69), it follows that

$$q_2^{(1)}(t_*) = \frac{\nu(2\omega)}{8}A_1^2\exp(2i\omega t_*) + \text{c.c.}$$

where the function ν is given by (70). Making use of the above results and expanding to $O(\varepsilon_p^2)$, we then obtain the following second-order equations:

$$\alpha_0 \frac{d^2 x_2}{dt_*^2} + \delta_0 \frac{dx_2}{dt_*} + \gamma_0 x_2 + \frac{4a_0^3}{\mathrm{Re}_l R_0^3}\left[1 + \Lambda \frac{d}{dt_*}\right] q_1^{(2)}(t_*)$$

$$= \frac{P^2}{4}[\phi_0(\omega) + \phi_2(\omega)A_{1P}^2(\omega)\exp(2i\omega t_*) + \text{c.c.}], \tag{73a}$$

$$\left[1 + \mathrm{De}\frac{d}{dt_*}\right] q_1^{(2)}(t_*) = \left[1 + \lambda\mathrm{De}\frac{d}{dt_*}\right]\frac{dx_2}{dt_*}. \tag{73b}$$

The new coefficients in this system can be expressed as follows:

$$F_1^{(0)} = \left(1 + \frac{\Delta_\rho a_0}{R_0}\right)^{-1}\left(1 + \frac{\Delta_\rho a_0^4}{R_0^4}\right), \tag{74a}$$

$$\phi_0(\omega) = \frac{(1 + \Lambda^2\omega^2)}{[D^2(\omega) + \omega^2\delta^2(\omega)]}\left[2\gamma_1 - \frac{\rho_{s0}}{\rho_{l0}}\left(1 + \frac{\Delta_\rho a_0^4}{R_0^4}\right)\omega^2\right.$$

$$\left. + \frac{20a_0^6\mathrm{De}(1 - \lambda)\omega^2}{\mathrm{Re}_l R_0^6(1 + \mathrm{De}^2\omega^2)}\right], \tag{74b}$$

$$\phi_2(\omega) = \gamma_1 + i\delta_1\omega + \alpha_1\omega^2 - \frac{i\rho_{s0}}{\rho_{l0}}\left(1 + \frac{\Delta_\rho a_0^4}{R_0^4}\right)\Lambda\omega^3$$

$$- \frac{2(1 + 2i\Lambda\omega)\nu(2\omega)a_0^3}{\mathrm{Re}_l R_0^3}\left(2 - \frac{a_0^3}{2R_0^3}\right) + \frac{4a_0^3\nu(\omega)}{\mathrm{Re}_l R_0^3}$$

$$\times\left[\frac{5a_0^3}{2R_0^3} - 2i\Lambda\omega\left(F_1^{(0)} - \frac{5a_0^3}{2R_0^3}\right)\right] + \frac{2\Lambda F_1^{(0)}\omega}{A_{1P}(\omega)}, \tag{74c}$$

$$\alpha_1 = \frac{\rho_{s0}}{\rho_{l0}}\left[\frac{5}{2} + \frac{4\Delta_\rho a_0}{R_0} - \frac{3\Delta_\rho a_0^4}{2R_0^4}\right.$$

$$\left. - \frac{8\Lambda}{\mathrm{Re}_s}\left(1 - \frac{a_0^3}{R_0^3}\right)\left(1 + \frac{3a_0^3}{R_0^3} - F_1^{(0)}\right)\right], \tag{74d}$$

$$\gamma_1 = \frac{3\kappa(3\kappa+1)}{2} - \sigma_1^* + \frac{\sigma_2^* a_0^4}{R_0^4}\left(1 - \frac{2a_0^3}{R_0^3}\right)$$

$$+ 4G_s^*\left(1 - \frac{a_0^3}{R_0^3}\right)\left[1 + \frac{3a_0^3}{R_0^3} + Z\left(1 + \frac{9a_0^6}{R_0^6}\right)\right], \tag{74e}$$

$$\delta_1 = \frac{4\rho_{s0}}{\rho_{l0}\mathrm{Re}_s}\left(1 - \frac{a_0^3}{R_0^3}\right)\left(1 + \frac{3a_0^3}{R_0^3}\right) + 2\Lambda(\gamma_1 - F_1^{(0)}\gamma_0). \tag{74f}$$

Evidently, the solution of (73) is a sum of zeroth and second harmonics

$$\begin{bmatrix} x_2(t_*) \\ q_1^{(2)}(t_*) \end{bmatrix} = \begin{bmatrix} A_0 \\ Q_0 \end{bmatrix} + \frac{1}{2}\begin{bmatrix} A_2 \\ Q_2 \end{bmatrix}\exp(2i\omega t_*) + \text{c.c.} \tag{75}$$

Again A_0, A_2, Q_0, Q_2 are the amplitudes that may depend on the angular frequency ω. Substituting solution (75) into Eqs. (73), we obtain the relationships $Q_2 = \nu(2\omega)A_2$ and $Q_0 = 0$ and the formulas for the zeroth- and second-harmonic amplitudes A_0 and A_2 of bubble oscillations:

$$\frac{A_0}{P^2} = \frac{\phi_0(\omega)}{4\gamma_0}, \quad \frac{A_2}{P^2} \equiv A_{2P}(\omega) = \frac{\phi_2(\omega)A_{1P}^2(\omega)}{2[D(2\omega) + 2i\omega\delta(2\omega)]}. \tag{76}$$

B. Resonance frequency and scattering cross sections

Many investigators on bubble dynamics neglect the effects of viscosity and other dissipative effects on the resonance frequency of bubble oscillation. Most (see for instance Ref. 8) assume that this frequency is equal to the *undamped* natural frequency f_0 despite the fact that the *damped* natural frequency f_n differs both from f_0 and from the resonance frequency f_{res} when damping is allowed for. (Here, we define f_0 as the frequency of undamped unforced oscillations, f_n as that for damped unforced oscillations, f_{res} as the forcing frequency which results in the maximum response amplitude for the damped bubble.) Let us consider the first-harmonic response function, i.e., the absolute value of the function $A_{1P}(\omega)$

$$\left|\frac{A_1}{P}\right| = |A_{1P}(\omega)| = \left[\frac{1 + \Lambda^2\omega^2}{D^2(\omega) + \omega^2\delta^2(\omega)}\right]^{1/2}. \tag{77}$$

If the liquid and the shell are inviscid, $\delta(\omega)$ is equal to zero and the amplitude of bubble oscillation goes to infinity (i.e., resonance takes place) at $\omega = \omega_{\mathrm{res0}}$ such that $D(\omega_{\mathrm{res0}}) = 0$. The same condition holds for free oscillations, i.e., the dimensional resonance frequency $f_{\mathrm{res0}} = U\omega_{\mathrm{res0}}/(2\pi a_0)$ is equal to the natural frequency $f_0 = U\omega_0/(2\pi a_0)$ in the case of undamped oscillation

$$f_{\mathrm{res0}} = f_0 = \frac{1}{2\pi a_0}\left[\frac{p_0\gamma_0}{\rho_{s0}(1 + \Delta_\rho a_0/R_0)}\right]^{1/2}. \tag{78}$$

In a viscous liquid the bubble resonates at the frequency $f_{\mathrm{res}} = U\omega_{\mathrm{res}}/(2\pi a_0)$ that is always less than f_{res0}. The nondimensional angular resonance frequency ω_{res} is the point at which the function $|A_{1P}(\omega)|$ has its maximal value. This point is one of the roots of the equation (the extremum condition)

$$\frac{d|A_{1P}(\omega)|}{d\omega} = 0. \tag{79}$$

If $\mathrm{De} > 0$ and $0 < \lambda < 1$, the left-hand side of Eq. (79) reduces to a polynomial of degree five in ω^2, and hence it does not have analytical solutions. Thus, in the viscoelastic liquid case the resonance frequency of bubble oscillations can only be found by the numerical maximization of the function $|A_{1P}(\omega)|$ (see the next section). However, it is possible to find the roots of Eq. (79) analytically if $\lambda = 1$. We then have a quadratic equation in ω^2

$$\Lambda^2\alpha_\mu^2\omega^4 + 2\alpha_\mu^2\omega^2 - (2\alpha_\mu\gamma_0 - \delta_\mu^2 + \Lambda^2\gamma_0^2) = 0,$$

$$\alpha_\mu = \alpha_0 + \frac{4a_0^3\Lambda}{\mathfrak{R}_l R_0^3}, \quad \delta_\mu = \delta_0 + \frac{4a_0^3}{\mathrm{Re}_l R_0^3}. \tag{80}$$

If

$$\delta_\mu > \delta_{\mu c} = (2\alpha_\mu\gamma_0 + \Lambda^2\gamma_0^2)^{1/2}, \tag{81}$$

Eq. (80) does not have real roots, and hence the bubble does not resonate at all. Otherwise, ω_{res} is given by the positive real root of (80). Upon neglecting the liquid compressibility ($\Lambda = 0$), the dimensional resonance frequency is found to be

$$f_{\mathrm{res1}} = \left\{ f_0^2 - \frac{2p_0}{\pi^2 a_0^2\rho_{l0}}\left(1 + \frac{\Delta_\rho a_0}{R_0}\right)^{-2} \right.$$

$$\left. \times\left[\frac{1}{\mathrm{Re}_s}\left(1 - \frac{a_0^3}{R_0^3}\right) + \frac{\rho_{l0}}{\rho_{s0}\mathrm{Re}_l}\frac{a_0^3}{R_0^3}\right]^2 \right\}^{1/2}. \tag{82}$$

As follows from (80), the encapsulated microbubble pulsates in a *compressible* viscous liquid resonantly at the frequency

$$f_{\mathrm{res2}} = \frac{1}{2\pi a_0\Lambda}\left(\frac{p_0}{\rho_{l0}}\right)^{1/2}$$

$$\times\left\{1 + \left[1 + \frac{\Lambda^2}{\alpha_\mu^2}(2\gamma_0\alpha_\mu - \delta_\mu^2 + \Lambda^2\gamma_0^2)\right]^{1/2}\right\}^{1/2}. \tag{83}$$

At the same time, the natural frequency $f_n = U\omega_n/(2\pi a_0)$ of bubble oscillations is generally defined from the condition $D(\omega) + i\omega\delta(\omega) = 0$ with ω being a *complex* variable: $\omega = \omega_n + i\omega_i$ (the imaginary part ω_i describes attenuation of free bubble oscillations with time, the real part ω_n is the nondimensional angular natural frequency). Even if the liquid is considered to be viscous and incompressible, f_n is not equal to the resonance frequency

$$f_n = \left\{ f_{\mathrm{res1}}^2 + \frac{p_0}{\pi^2 a_0^2\rho_{l0}}\left(1 + \frac{\Delta_\rho a_0}{R_0}\right)^{-2} \right.$$

$$\left. \times\left[\frac{1}{\mathrm{Re}_s}\left(1 - \frac{a_0^3}{R_0^3}\right) + \frac{\rho_{l0}}{\rho_{s0}\mathrm{Re}_l}\frac{a_0^3}{R_0^3}\right]^2 \right\}^{1/2}. \tag{84}$$

Of particular interest for ultrasound contrast imaging is calculation of scattering cross sections σ_{s1} and σ_{s2} by the encapsulated microbubble at the driving (fundamental) frequency $f = U\omega/(2\pi a_0)$ and at twice the driving frequency $2f$, respectively. These scattering cross sections (which have dimensions of area) are related to the ratio of the total acous-

tic power scattered by the bubble at the first and second harmonics to the intensity of the incident acoustic field[5]

$$\sigma_{s1} = \frac{4\pi a_0^2 r_*^2 I_1}{I_0}, \quad \sigma_{s2} = \frac{4\pi a_0^2 r_*^2 I_2}{I_0}, \tag{85}$$

where $I_1 = |P_{s1}|^2/(2\rho_l C_l)$ and $I_2 = |P_{s2}|^2/(2\rho_l C_l)$ are the intensities of the scattered acoustic wave at the first and second harmonics, $I_0 = p_0^2 P_A^2/(2\rho_l C_l) = \varepsilon_p^2 p_0^2 P^2/(2\rho_l C_l)$ is the intensity of the incident acoustic wave. Note that P_A or P is taken to be real. The P_{s1} and P_{s2} are the first- and second-harmonic amplitudes of the scattered wave. As seen from (46), the scattered pressure field is $p_s(t_*, r_*) = -p_0 Q'(t_* - Mr_*)/r_*$. Because the amplitude of bubble oscillation is small, we can expand p_s in powers of the small parameter ε_p

$$p_s(t_*, r_*) = -\frac{p_0}{3r_*} \frac{d^2 a_*^3(\xi)}{d\xi^2}$$

$$\approx -\varepsilon_p \frac{d^2 x_1(\xi)}{d\xi^2}$$

$$-\varepsilon_p^2 \frac{d^2}{d\xi^2}[x_2(\xi) + x_1^2(\xi)] - O(\varepsilon_p^3),$$

$$\xi = t_* - Mr_*. \tag{86}$$

Substituting (69) and (75) into (86) yields

$$p_s(t_*, r_*) = \frac{P_{s1}}{2} \exp i\omega t_* + \frac{P_{s2}}{2} \exp 2i\omega t_* + \text{c.c.},$$

where

$$P_{s1} = \varepsilon_p \omega^2 p_0 A_1 \frac{\exp(-ikr_*)}{r_*},$$

$$P_{s2} = 4\varepsilon_p^2 \omega^2 p_0 \left(A_2 + \frac{A_1^2}{2}\right) \frac{\exp(-2ikr_*)}{r_*}, \quad k = \omega M. \tag{87}$$

Finally, insertion of Eqs. (87), (71) and the second equation in (76) into Eq. (85) gives the following expressions for the scattering cross sections at the first and second harmonics:

$$\sigma_{s1} = 4\pi a_0^2 \omega^4 |A_{1P}(\omega)|^2,$$

$$\sigma_{s2} = 64\pi a_0^2 P_A^2 \omega^4 \left|A_{2P}(\omega) + \frac{A_{1P}^2(\omega)}{2}\right|^2$$

$$= 16\pi a_0^2 P_A^2 \omega^4 |A_{1P}|^4 \Gamma, \tag{88}$$

where

$$\Gamma = \left|1 + \frac{\phi_2(\omega)}{D(2\omega) + 2i\omega\delta(2\omega)}\right|^2. \tag{89}$$

The first expression of (88) is consistent with Church's derivation [see formula (26a) in Ref. 5]. However, the formula for the second-harmonic scattering cross section [(26b) in Ref. 5] was in error because it did not take into account the nonlinear relationship between the pressure field scattered by the bubble and radial oscillations of the bubble.

V. RESULTS AND DISCUSSIONS

In this section, we calculate the total damping coefficient, the resonance frequency, and the scattering cross sections for the air-filled encapsulated bubble in blood. In all calculations the unperturbed liquid pressure $p_0 = 0.1$ MPa,

the liquid and solid densities $\rho_{l0} = 998$ kg m^{-3} and $\rho_{s0} = 1100$ kg m^{-3}, the interfacial tensions $\sigma_1 = 0.04$ kg s^{-2} and $\sigma_2 = 0.005$ kg s^{-2}, the liquid viscosity is equal to the high-shear-rate viscosity of blood: $\mu_l = 0.004$ kg m^{-1} s^{-1} (see Ref. 40), and the retardation time $\lambda_2 = 0$ s. The inner radius of the microbubble a_0 and the shell thickness $d = R_0 - a_0$ are varied from 1 to 5 μm and from 15 to 200 nm, respectively. The values of the speed of sound in the liquid, the relaxation time, and the shell viscosity and elasticity are $C_l = \infty$ (incompressible case), 1500, and 500 m s^{-1}, $\lambda_1 = 0$ (Newtonian liquid), 0.01, 0.1, and 1 μs, $\mu_s = 0.5$, 1.77, and 5 kg m^{-1} s^{-1}, $G_s = 15$, 88.8, and 150 MPa.

The values chosen for the parameters are in line with the experimental data for ultrasound contrast agents. Specifically, such microbubbles are restricted to have a size between 1 and 10 μm.[48] The larger bubbles cannot pass through the pulmonary circulation. The scattered field from the smaller bubbles is extremely small.[48,49] This directly follows from the formulas for scattering cross sections (88): σ_{s1} and $\sigma_{s1} \sim a_0^6 \Omega^4$, i.e., at given driving frequency the acoustic response from a larger bubble is higher. The thickness of the shell around the microbubbles depends on their size[8] and the type of surface-active material. Albunex® bubbles are covered by the shell of approximately 15 nm in thickness.[5,50] Quantison™ bubbles have the thickest shell ($d = 200$ nm).[7] It should be noted that there are no direct measurements of the shell viscosity and elasticity for ultrasound contrast agents. The shell viscosity is estimated, for example, by fitting the experimental data for the attenuation of acoustic signals in the microbubble suspension to the predictions of the simplistic theoretical model of de Jong.[4,51] Also, these parameters may depend on the shell thickness[15] and other factors. We therefore consider different values of the shell viscosity and elasticity. Nevertheless, the second choice ($\mu_s = 1.77$ kg m^{-1} s^{-1} and $G_s = 88.8$ MPa) corresponds to empirical values for de Jong's shell stiffness and shell damping parameters.[4,5] The values of the interfacial tensions and densities are the same as in Ref. 5. Due to the presence of nucleation agents and/or other microbubbles of contrast-agent suspension, blood surrounding an encapsulated microbubble provides a medium which is more compressible than blood free of bubbles. This is the reason why we choose the value 500 m/s for the sound speed in the liquid.

Our expectation that the 4-constant Oldroyd constitutive equation (with the nonzero relaxation and retardation times) can provide reasonable predictions for the radial (diverging-converging) flow of blood in large vessels (and of dilute polymer solutions) induced by high-frequency oscillations of a gas microbubble is based on the following facts:

(i)   Blood is a fluidized suspension of small elastic cells (red cells, white cells, platelets) surrounded by blood plasma. The cell deformability and aggregation result in the stress relaxation and well-documented shear thinning of blood at small and moderate shear rates.[12,52–55] Plasma by itself is a colloidal suspension of proteins in an electrolyte solution, which shows small deviation from the behavior of a pure liquid, at least in some patients suffering from leukemia.[56,57]

(ii)　Due to complex structure, neither whole blood nor blood plasma is a Newtonian liquid, even though viscometric observations show negligible deviations from the Newtonian law, as for instance, in the case of blood flow in large vessels.[40] The modern viscometric techniques operate at the shear rates (less than $30\,000$ s^{-1}) which are not enough to determine the small elasticity, corresponding, for example, to the relaxation time of the order of a microsecond. The most experimental data on blood viscosity have been obtained at shear rates less than $12\,000$ s^{-1} (see Refs. 52, 58, and 59). Blood viscosity has also been measured using oscillatory flow apparatus operated at the frequency of several Hz.[60–62] However, the characteristic time for the radial flow around the resonantly pulsating bubble of radius 1 μm is less than a microsecond. In particular, if the equilibrium liquid pressure $p_0 = 0.1$ MPa, liquid density $\rho_{l0} = 10^3$ kg/m^3, and bubble radius $a_0 = 1$ μm, the characteristic time $t_* = a_0/\sqrt{p_0/a_0} = 0.1$ μs. Even small elasticity may, therefore, affect the bubble pulsations because the Deborah number $De = \lambda_1/t_*$ is of the order of unity, if the relaxation time $\lambda_1 = 0.1$ μs. Incidentally, this fact allows the use of a gas microbubble for the measurement of very small elasticity of the liquid: the acoustic field scattered by the bubble in a Newtonian liquid will be different from that in a slightly viscoelastic liquid. It is worth noting that such ultrasonic spectrometry is already used in food engineering.[63]

(iii)　Rheological behavior of blood in large vessels has been investigated using the Oldroyd constitutive equations, among which are the 4-constant Oldroyd,[64,65] 5-constant Oldroyd,[66] and Oldroyd-B models.[67,68] As shown by Chmiel and Walitza,[65] there is a good agreement between the predictions of the 4-constant Oldroyd model and experimental data under the assumption that the parameters of the model are functions of invariants of the rate-of-strain tensor. This model can also be used for blood-mimicking materials utilized to testing medical ultrasound techniques[69–71] and for suspensions of normal red blood cells in albumin, in which the cell aggregates are not formed and elasticity is only due to the cell deformation.[52]

(iv)　The fact that the relaxation and retardation times decrease with increasing shear rate directly follows from the experimental data on the aggregation and disaggregation of red blood cells in shear flow.[72] As noted by Cokelet,[53] the characteristic time for red cell aggregation is of the order of 1 min in the absence of superimposed shear but becomes of the order of 10 s at a shear rate of about 10 s^{-1}. At high shear rates, the relaxation time is expected to be determined by the red cell deformation which gives the values below 0.06 s.

(v)　Not only do blood viscosity and elasticity affect the dynamics of microbubbles in blood vessels, but also the viscoelastic properties of surrounding tissues (in particular, blood vessel walls) may have some impact on microbubble oscillations. The tissue viscoelasticity should be taken into account if the distance between the microbubble center and the tissue does not exceed the wavelength of acoustic waves. In that case, tissue will be located in either the internal or intermediate zones (see Sec. III). To calculate the shear stress tensor $\boldsymbol{\tau}^{(l)}$ in these zones and the term $q(t_*)$ of Eqs. (63), we then need to assume that the liquid surrounding the microbubble is a medium consisting of both blood and tissue. For the problem of bubble oscillation, the 4-constant Oldroyd model is a good first step in trying to account for viscoelastic effects in such medium. It should be noted that the radial oscillations of a gas bubble in tissue by itself have already been investigated using the Upper-Convective Maxwell and linear Jeffreys models.[46,74,73]

At a shear rate of about 1500 s^{-1}, the apparent blood viscosity is about 0.004 kg m^{-1}s^{-1} (see Ref. 52). According to existing experimental results, it does not change at further increasing shear rate.[40] However, modern viscometric techniques are not capable of determining the small elasticity of blood (in large vessels), which may affect the microbubble pulsations. One can model this small elasticity as well as the elasticity of surrounding tissue by adding elastic terms to the Newtonian constitutive equation with the high-shear-rate viscosity of 0.004 kg m^{-1} s^{-1}. This should work if the characteristic time for bubble pulsation is much less than the characteristic time for shear flow at which the well-documented shear thinning takes place (from 1/1500 s to 10 s), because our purpose is not to consider elastic effects due to cell aggregation. We would like only to understand how small blood elasticity (for example, plasma elasticity) or/and tissue elasticity affects microbubble pulsations under the conditions when blood is usually considered to be Newtonian. This is why we analyze bubble oscillations assuming that the zeroth order shear viscosity in the constitutive equation is equal to 0.004 kg m^{-1} s^{-1}. We neglect the retardation term in the constitutive equation ($\lambda_2 = 0$) for the sake of simplicity. From Eqs. (72) it follows that the only effect of the rate-of-strain relaxation is a decrease in the contribution from liquid elasticity to bubble pulsations.

A. Damping coefficients

In order to obtain the correct expressions for linear damping coefficients, one needs to divide both the numerator and denominator of (71) by $1 + i\Lambda\omega$ and turn back to dimensional variables. The formula for the first-harmonic amplitude $A_{1d} = a_0 A_1$ then takes the form

$$A_{1d} = a_0 P A_{1P}(\Omega)$$
$$= -\frac{ip_0 P}{\rho_{s0} a_0 (1 + \Delta_\rho a_0/R_0)}$$
$$\times \left[\frac{1}{\Omega_0^2 - \Omega^2 + S_{\text{ac}}(\Omega) + S_{\text{el}}(\Omega) + 2i\Omega\beta(\Omega)}\right]. \quad (90)$$

Here $\Omega = (a_0^{-1}\sqrt{p_0/\rho_{l0}})\omega$ is the angular driving frequency, $\Omega_0 = (a_0^{-1}\sqrt{p_0/\rho_{l0}})\omega_0 = 2\pi f_0$ is the angular undamped natural frequency, Δ_ρ is given by (42), and

$$S_{ac}(\Omega) = \frac{\rho_{l0}^2}{\rho_{s0}^2}\left(1 + \frac{\Delta_\rho a_0}{R_0}\right)^{-2}\frac{\Omega^4 a_0^2}{C_l^2}$$

$$\times\left[1 + \frac{\rho_{l0}^2}{\rho_{s0}^2}\left(1 + \frac{\Delta_\rho a_0}{R_0}\right)^{-2}\frac{\Omega^2 a_0^2}{C_l^2}\right]^{-1}, \quad (91a)$$

$$S_{el}(\Omega) = \frac{4\mu_l a_0}{\rho_{s0}R_0^3}\left(1 + \frac{\Delta_\rho a_0}{R_0}\right)^{-1}\frac{(\lambda_1 - \lambda_2)\Omega^2}{1 + \lambda_1^2\Omega^2}, \quad (91b)$$

are functions of Ω which can be interpreted as contributions of acoustic radiation and elasticity of the liquid to the stiffness of the bubble. The total damping coefficient $\beta(\Omega)$ that also depends on the driving frequency is the sum of four components: $\beta(\Omega) = \beta_{vis1} + \beta_{vis2} + \beta_{ac}(\Omega) - \Delta\beta_{el}(\Omega)$, where

$$\beta_{vis1} = \frac{2\mu_l}{\rho_{s0}a_0^2}\left(1 + \frac{\Delta_\rho a_0}{R_0}\right)^{-1}\frac{a_0^3}{R_0^3}, \quad (92a)$$

$$\beta_{vis2} = \frac{2\mu_s}{\rho_{s0}a_0^2}\left(1 + \frac{\Delta_\rho a_0}{R_0}\right)^{-1}\left(1 - \frac{a_0^3}{R_0^3}\right), \quad (92b)$$

$$\beta_{ac}(\Omega) = \frac{\rho_{l0}}{\rho_{s0}}\left(1 + \frac{\Delta_\rho a_0}{R_0}\right)^{-1}\frac{\Omega^2 a_0}{2C_l}$$

$$\times\left[1 + \frac{\rho_{l0}^2}{\rho_{s0}^2}\left(1 + \frac{\Delta_\rho a_0}{R_0}\right)^{-2}\frac{\Omega^2 a_0^2}{C_l^2}\right]^{-1}, \quad (92c)$$

$$\Delta\beta_{el}(\Omega) = \frac{2\mu_l a_0}{\rho_{s0}R_0^3}\left(1 + \frac{\Delta_\rho a_0}{R_0}\right)^{-1}\frac{\lambda_1(\lambda_1 - \lambda_2)\Omega^2}{1 + \lambda_1^2\Omega^2}, \quad (92d)$$

are the liquid and shell parts of the viscous damping coefficient, the acoustic radiation damping coefficient, and the contribution of the liquid elasticity to $\beta(\Omega)$, respectively. Note that thermal effects were ignored upon deriving (71). In the case of a free bubble ($\rho_{l0} = \rho_{s0}$, $a_0 = R_0$), when $\Delta_\rho = \beta_{vis2} = 0$, the viscous and acoustic radiation damping coefficients are identical to those derived by Prosperetti:[28]

$$\beta_{vis} = \beta_{vis1} = \frac{2\mu_l}{\rho_{l0}a_0^2}, \quad \beta_{ac}(\Omega) = \frac{\Omega^2 a_0}{2C_l}\left[1 + \left(\frac{\Omega a_0}{C_l}\right)^2\right]^{-1}, \quad (93)$$

and the acoustic contribution to the bubble stiffness, $S_{ac}(\Omega)$, is equal to the third term in the right-hand side of Eq. (12) in Ref. 28

$$S_{ac}(\Omega) = \frac{\Omega^4 a_0^2}{C_l^2}\left[1 + \frac{\Omega^2 a_0^2}{C_l^2}\right]^{-1}. \quad (94)$$

It should be mentioned that the formulas for the viscous damping coefficients (92a) and (92b) are equivalent to Church's expressions [(30a) and (30b) in Ref. 5]. However, if the shell and the liquid have different densities, as was assumed by Church, the acoustic radiation damping coefficient β_{ac} differs from that for a free bubble and formula (30d) of Ref. 5 is, therefore, inexact in that case. Note that the liquid compressibility should be taken into account for small bubbles at high (natural) frequencies. The fact is that both the acoustic contribution to the bubble stiffness S_{ac} in Eq. (91a) and the acoustic radiation damping coefficient β_{ac} in (92c) increase with decreasing the bubble radius a_0 under the assumption that $\Omega = \Omega_0$, $\rho_{l0} = \rho_{s0}$, and the shell thickness $d = R_0 - a_0$ is fixed.

From (90) and the condition $\lambda_1 > \lambda_2$ it follows that elasticity of the liquid enhances the stiffness of the bubble and reduces viscous damping of bubble oscillation. However, $\Delta\beta_{el}(\Omega)$ is always less than β_{vis1}, i.e., viscous damping cannot be canceled even in the case of large relaxation times. Hereafter, we consider $\beta_{vis1} - \Delta\beta_{el}(\Omega)$ as a liquid viscous damping coefficient and β_{vis2} as a shell viscous damping coefficient. Elasticity of the shell raises the stiffness of the bubble through an increase in the undamped natural frequency, and yet it does not influence damping. Also, oscillations of encapsulated microbubbles highly depend on the difference in density between the shell and the liquid. If the shell is more dense than the liquid ($\rho_{l0}/\rho_{s0} < 1$), the amplitude and attenuation of encapsulated-microbubble oscillations are smaller than those of free-microbubble oscillations.

As noted above, the effects of heat conduction through the microbubble walls can be incorporated in analysis of microbubble oscillation by considering the polytropic exponent κ instead of a ratio of specific heats for the gas γ_g and by accounting for the thermal dissipation in the linear damping coefficient. The $\beta(\Omega)$ is then equal to

$$\beta(\Omega) = \beta_{vis1} + \beta_{vis2} + \beta_{ac}(\Omega) + \beta_T(\Omega) - \Delta\beta_{el}(\Omega), \quad (95)$$

where $\beta_T(\Omega)$ is the frequency-dependent thermal damping coefficient. We take into account thermal effects by reference to the expressions for κ and $\beta_T(\Omega)$ given by Prosperetti[29] for small-amplitude oscillations of free gas bubbles. There are no effects of encapsulation on the polytropic exponent if the specific heats of the shell are very large compared with those of the gas, and therefore,

$$\kappa = \frac{1}{3}\text{Real}\{\tilde{F}(i\text{Pe}_g/2)\} = \frac{\gamma_g[1 + 3(\gamma_g - 1)G_-(\sqrt{\text{Pe}_g})]}{[1 + 3(\gamma_g - 1)G_-(\sqrt{\text{Pe}_g})]^2 + 9(\gamma_g - 1)^2[G_+(\sqrt{\text{Pe}_g}) - 2/\text{Pe}_g]^2}. \quad (96)$$

Here γ_g is the ratio of constant-pressure to constant-volume specific heats for the gas, $\tilde{F}(i\text{Pe}_g/2)$ is given in Eq. (3.28) of Ref. 29,

$$\text{Pe}_g = \frac{2\Omega a_0^2}{\nu_g} = \frac{2\Omega\rho_g c_g a_0^2}{k_g} \quad (97)$$

is the Peclet number for the gas, ν_g the thermal diffusivity of the gas, k_g the thermal conductivity of the gas, c_g the specific heat of the gas at constant pressure, and

$$G_{\pm}(\sqrt{Pe_g}) = \frac{1}{\sqrt{Pe_g}}\left[\frac{\sinh\sqrt{Pe_g} \pm \sin\sqrt{Pe_g}}{\cosh\sqrt{Pe_g} - \cos\sqrt{Pe_g}}\right].$$

As with the damping coefficient due to the liquid viscosity β_{vis1}, the thermal damping coefficient $\beta_T(\Omega)$ for encapsulated microbubble oscillations differs from that for free bubble oscillations by the factor $\rho_{l0}/[\rho_{s0}(1+\Delta_\rho a_0/R_0)]$

$$\beta_T(\Omega) = \frac{p_0}{2\rho_{s0}a_0^2}\left(1+\frac{\Delta_\rho a_0}{R_0}\right)^{-1}\frac{Im\{\widetilde{F}(iPe_g/2)\}}{\Omega}$$

$$= \frac{9p_0\gamma_g(1+\Delta_\rho a_0/R_0)^{-1}[G_+(\sqrt{Pe_g})-2/Pe_g]}{2\rho_{s0}a_0^2(\gamma_g-1)\Omega\{[3G_-(\sqrt{Pe_g})+1/(\gamma_g-1)]^2+9[G_+(\sqrt{Pe_g})-2/Pe_g]^2\}}. \tag{98}$$

Figure 3 illustrates the dependence of the total damping coefficient $\beta(\Omega)$ as well as the liquid viscous, shell viscous, acoustic radiation, and thermal damping coefficients [$\beta_{vis1} - \Delta\beta_{el}(\Omega)$, β_{vis2}, $\beta_{ac}(\Omega)$, $\beta_T(\Omega)$] on the driving frequency Ω for the encapsulated bubble of radius $a_0 = 1$ μm in accordance with Eqs. (92), (95), and (98). The liquid surrounding the microbubble is considered to be viscoelastic with the relaxation time $\lambda_1 = 0.1$ μs. The shell around the microbubble is thin ($d = 15$ nm) and very viscous [$\mu_s = 1.77$ kg/(m·s)]. The total damping of such microbubbles, as discussed by Church,[5] is dominated by viscous effects. Indeed, in the range of medical ultrasound frequencies ($f = 1-10$ MHz) thermal damping is three orders of magnitude less than viscous damping due to the shell. While radiation damping rises with increasing the driving frequency, it comes into play only at frequencies above 10 MHz. When comparing the liquid and shell contributions to viscous damping, one can see that $\beta_{vis1} \gg \beta_{vis2}$ if

$$\mu_s \gg \mu_l\left(\frac{R_0^3}{a_0^3}-1\right)^{-1}.$$

This gives $\mu_s \gg 22\mu_l$ for a microbubble of radius 1 μm with a 15 nm thick shell. For the above values of viscosities ($\mu_s/\mu_l = 442.5$) the total damping of microbubble oscillations is determined practically by the shell parameters even if the liquid is Newtonian. Obviously, the β_{vis1} and the difference between β_{vis1} and β_{vis2} become greater with increasing the shell thickness, i.e., one can neglect liquid viscous, thermal, and radiation effects when considering the attenuation of oscillations for ultrasound contrast agents with thicker shells (Fig. 4). Moreover, if the liquid is viscoelastic, the liquid viscous damping drops sharply as the driving frequency increases (Fig. 3). This happens even at small relaxation times ($\lambda_1 \geq 0.1$ μs) when elastic effects seem to be negligible (Fig. 5). From (92d) it follows that the liquid elasticity has a minor effect on viscous damping if $\lambda_1 \ll 1/(2\pi f)$. This gives $\lambda_1 < 0.01$ μs for the frequencies be-
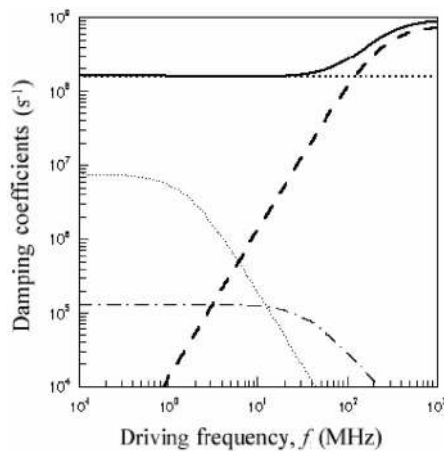

FIG. 3. Damping coefficients versus driving frequency for an encapsulated air bubble of radius 1 μm. The solid line is the total damping coefficient β. The dashed and dash–dot lines correspond to the acoustic radiation and thermal damping coefficients β_{ac} and β_T, the thick and thin dotted lines are the shell and liquid viscous damping coefficients $\beta_{vis1} - \Delta\beta_{el}$ and β_{vis2}. Parameters: $p_0 = 0.1$ MPa, $d = R_0 - a_0 = 15$ nm, $\mu_l = 0.004$ kg/(m·s), $\mu_s = 1.77$ kg/(m·s), $\lambda_1 = 0.1$ μs, $\lambda_2 = 0$ s, $\rho_{l0} = 998$ kg/m³, $\rho_{s0} = 1100$ kg/m³, $C_l = 1500$ m/s, $\sigma_1 = 0.04$ kg/s², $\sigma_2 = 0.005$ kg/s².

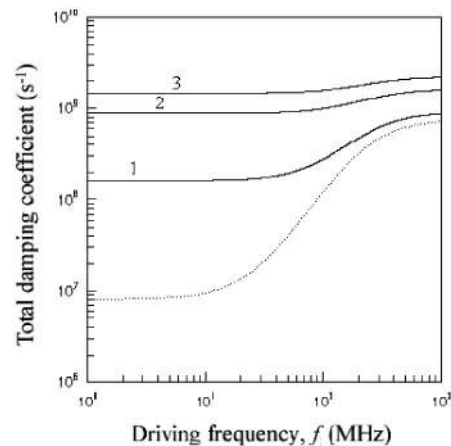FIG. 4. Total damping coefficient as a function of driving frequency for an encapsulated microbubble of radius 1 μm. The curves labeled 1–3 are for values of shell thickness $d = 15$, 100, and 200 nm, respectively. The total damping coefficient for a free microbubble of the same radius is marked off by the dashed line.
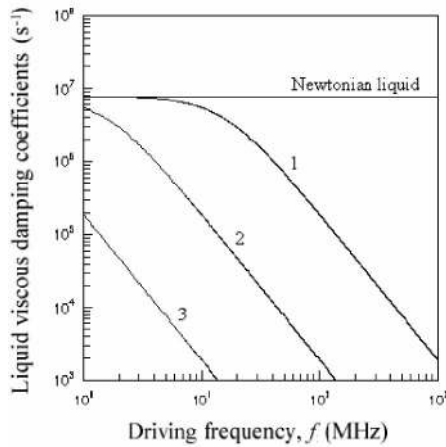
FIG. 5. Liquid viscous damping coefficient as a function of driving frequency for an encapsulated microbubble in a viscoelastic liquid with different values of the relaxation time. The curves labeled 1–3 are for values of the relaxation time $\lambda_1 = 0.01$ μs, 0.1, and 1 μs, respectively. The remaining parameters are the same as in Fig. 3.
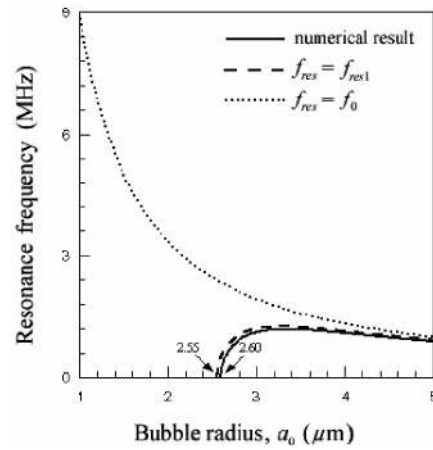

FIG. 6. Resonance frequency (solid) for an encapsulated microbubble in an incompressible Newtonian liquid, as a function of bubble radius, compared with the undamped natural frequency (dotted). The dashed line is the analytical solution (82). The shell elasticity is 15 MPa, $C_l = \infty$, $\lambda_1 = \lambda_2 = 0$ s. Other parameters are as in Fig. 3.

tween 1 and 10 MHz. All these suggest that viscosity of the shell is the most important parameter for defining the attenuation of microbubble oscillation.

B. Resonance frequency

In view of Eq. (90), the amplitude-frequency response function $|A_{1P}|$ can be written as

$$
\begin{aligned}
&|A_{1P}(\Omega)| \\
&= \frac{p_0}{\rho_{s0} a_0^2 (1 + \Delta_\rho a_0 / R_0)} \\
&\quad \times \left\{ \frac{1}{[\Omega_0^2 - \Omega^2 + S_{ac}(\Omega) + S_{el}(\Omega)]^2 + 4\Omega^2 \beta^2(\Omega)} \right\}^{1/2},
\end{aligned}
$$

(99)

where $\beta(\Omega)$ takes into account the thermal dissipation and is given by (95). Also, $\Omega_0 = 2\pi f_0$ is calculated according to the formula (78) wherein the polytropic exponent κ is given by Eq. (96). We perform the numerical maximization of the amplitude-frequency response function in order to find the resonance frequency f_{res} of bubble oscillation. The numerical results are shown in Figs. 6–8.

Previously, the resonance frequency f_{res} for the encapsulated microbubbles was taken to be equal to the undamped natural frequency f_0 (see Refs. 8 and 15). However, this works only for reasonably large bubbles, when the viscous damping coefficients are much less than the undamped natural frequency. The ratio of $\beta_{vis1} + \beta_{vis2}$ to f_0, and hence the difference between f_{res} and f_0 rise as the bubble size decreases. Numerical analysis confirms this. The resonance and undamped natural frequencies (solid and dotted lines) for the encapsulated microbubble in an incompressible Newtonian liquid ($C_l = \infty$, $\lambda_1 = \lambda_2 = 0$ s), as functions of the inner bubble radius, are depicted in Fig. 6. First, this figure shows that the assumption $f_{res} = f_0$ does not work for the encapsulated microbubble having a radius below 5 μm. Second,

there exists a critical radius a_{0c} such that any microbubble of radius $a_0 < a_{0c}$ does not resonate at all. The critical radius for the air-filled microbubble surrounded by blood and encapsulated by a 15 nm thick shell with elasticity of 15 MPa and viscosity of 1.77 kg m^{-1} s^{-1} is 2.6 μm. This value is above a mean bubble radius for many commercial contrast-agent suspensions.[48] Third, unlike the undamped natural frequency, the dependence of the resonance frequency on the bubble radius is not monotonic. There exists a maximal value of the resonance frequency. If the driving frequency exceeds this value, no bubbles oscillate resonantly. It immediately follows that for each value of the driving frequency below the maximal one there are two resonant bubble sizes (not one as before). It should be noted that the resonance frequency of bubble oscillation is not the frequency at which the scattering cross section has a local maximum (see the next section). The latter frequency is a monotonic function of the bubble radius which goes to infinity at the critical value of the radius.

Because the thermal damping coefficient is nearly constant and very small (compared with the viscous damping coefficients) for micron bubbles at medical ultrasound frequencies (Fig. 3), the resonance frequency is scarcely affected by the thermal dissipation. The analytical solution (82) with $\kappa = 1.1$, which is marked off by the dashed line in Fig. 6, differs from the numerical result only slightly. Note that if the liquid is considered to be incompressible and Newtonian, the only reason why the numerical solution may be different from the formula (82) is the thermal dissipation. For the parameters as in Fig. 6, the inclusion of thermal damping leads to an increase in the critical bubble radius from 2.55 to 2.6 μm (less than 2%). Upon neglecting thermal damping and elasticity of the liquid, the critical radius a_{0c} can be found analytically from (81) which, in view of (90), can be rewritten as follows:
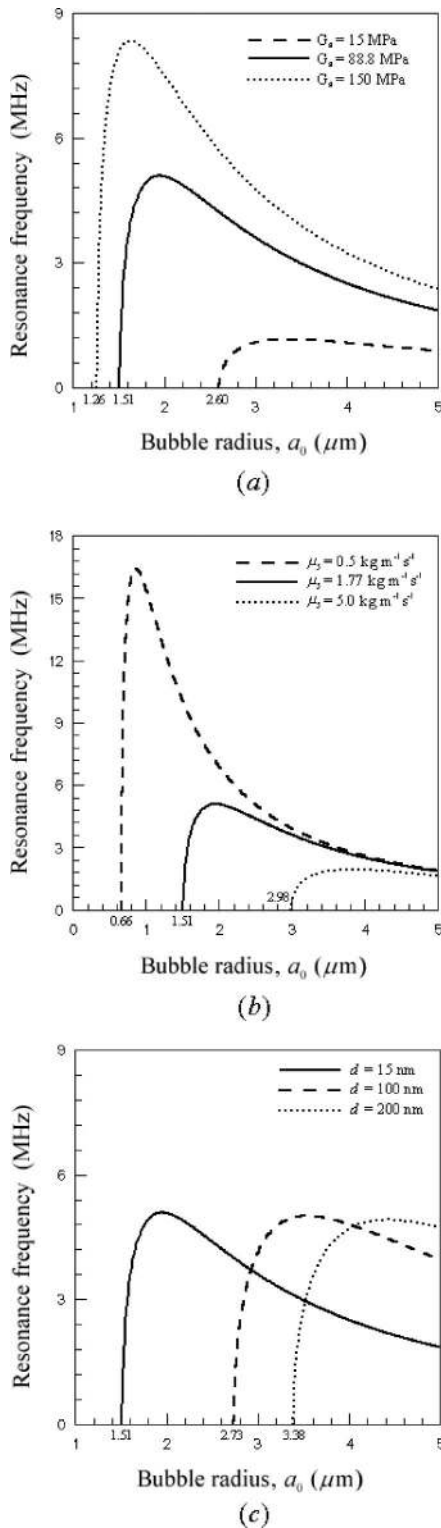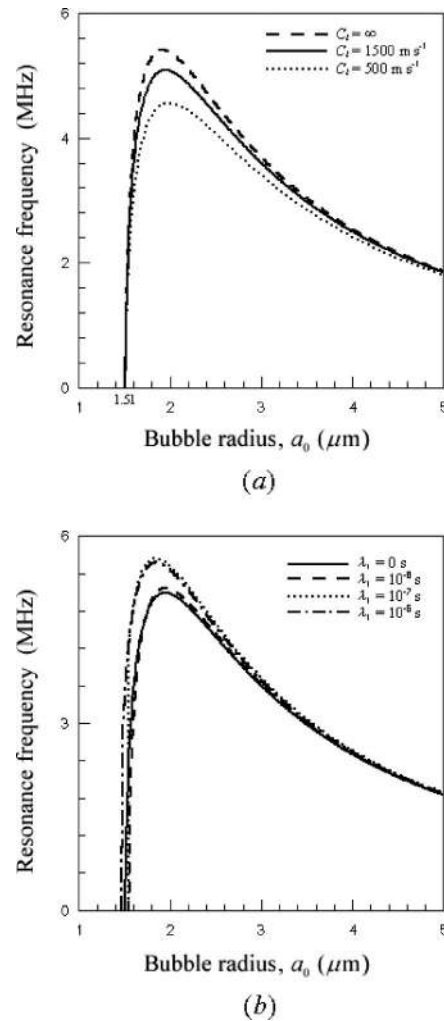
FIG. 8. Effects of liquid compressibility and viscoelasticity on the resonance frequency of microbubble oscillation. Plots (a) and (b) are resonance frequency as a function of bubble radius for different values of C_l at $\lambda_1 = \lambda_2 = 0$ s and of λ_1 at $C_l = 1500$ m/s and $\lambda_2 = 0$ s, respectively. The shell elasticity is 88.8 MPa, other parameters are as in Fig. 6.

FIG. 7. Resonance frequency versus bubble radius for an encapsulated microbubble in a compressible Newtonian liquid ($C_l = 1500$ m/s) for different values of (a) shell elasticity, (b) shell viscosity, and (c) shell thickness. For plots (a) and (c) $\mu_s = 1.77$ kg/(m·s); for (b) and (c) $G_s = 88.8$ MPa; for (a) and (b) $d = 15$ nm. Other parameters are given above.

The existence of resonant peaks in the experimental scattering cross section curves (at the driving frequency) for contrast-agent suspensions with a mean radius below 2.6 μm indicates that the value of the shell elasticity is more than 15 MPa and/or the value of the shell viscosity is less than 1.77 kg m^{-1} s^{-1}. As seen in Figs. 7(a) and 7(b), the critical bubble radius and the maximal value of the resonance frequency increase with increasing the shell elasticity and decreasing the shell viscosity. Also, the critical radius is larger for the microbubbles with thicker shells [Fig. 7(c)]. The fact that the critical bubble radius depends on the shell parameters gives us a possibility to evaluate one of them. For example, we can measure the shell thickness by atomic force microscopy[5] and the shell viscosity by fitting the experimental data for the ultrasound attenuation in the contrast-agent suspension to the theoretical calculations based on (95). Of course, we should sum $\beta(\Omega)$ over all available bubble sizes for this. Note that (95) includes the contribution of liquid elasticity to the total damping coefficient, which was not taken into account previously. Having these data and knowing the values of the gas and liquid parameters, we only need

$$\frac{2}{\rho_{s0} a_{0c}^2} \left(1 + \frac{\Delta_\rho}{1 + d/a_{0c}} \right)^{-1} \left[\mu_s - \frac{\mu_s - \mu_l}{(1 + d/a_{0c})^3} \right] = \frac{\Omega_0}{\sqrt{2}},$$

$$(100)$$

where Ω_0 is also a function of a_{0c}.

to find the critical bubble radius in order to evaluate the shell elasticity.

The effects of the liquid compressibility on the resonance frequency are small as compared to the shell effects. There is a decrease in the maximal resonance frequency and no change in the critical bubble radius with decreasing the speed of sound in the liquid [Fig. 8(a)]. Figure 8(a) shows that the resonance frequency of a 2-micron bubble equals about 4.15 MHz if the liquid is considered to be incompressible and equals about 4.11 MHz if the speed of sound C_l = 1500 m/s. Nonetheless, the difference 0.04 MHz cannot be considered very small (relative to experimental measurement sensitivity). The elasticity of the liquid influences the resonance frequency, though its effects are much smaller than the effects of the shell elasticity because $\mu_l \ll \mu_s$. In a viscoelastic liquid the maximal resonance frequency is always larger than in a Newtonian liquid [Fig. 8(b)]. The critical bubble size deviates slightly from the value obtained in the case of a Newtonian liquid. It is necessary to say that the liquid elasticity has the greatest impact on the resonance frequency at $\lambda_1 \sim 0.1$ μs [the dotted line in Fig. 8(c)]. The effects of the liquid elasticity are diminished with a further increase in λ_1 (compare the dotted and dash–dot lines).

C. Scattering cross sections

In order to incorporate thermal damping into the formula for the second-harmonic amplitude, we rewrite the second equation in (76) in the form

$$A_{2P}(\Omega) = \frac{\phi_2^*(\Omega) A_{1P}^2(\Omega)}{\Omega_0^2 - 4\Omega^2 + S_{ac}(2\Omega) + S_{el}(2\Omega) + 4i\Omega\beta(2\Omega)},$$
(101)

where

$$\phi_2^*(\Omega) = \frac{p_0}{\rho_{s0} a_0^2} \left(1 + \frac{\Delta_\rho a_0}{R_0}\right)^{-1} \frac{[1 - 2i(\Lambda a_0/U)\Omega]\phi_2(\Omega)}{1 + 4(\Lambda a_0/U)^2\Omega^2}.$$

The thermal damping coefficient β_T is inside $A_{1P}(\Omega)$ and $\beta(2\Omega)$. The first- and second-harmonic scattering cross sections σ_{s1} and σ_{s2} are then given by the following expressions:

$$\sigma_{s1} = \frac{4\pi\rho_{l0}^2 a_0^6}{p_0^2} \Omega^4 |A_{1P}(\Omega)|^2,$$
(102a)

$$\sigma_{s2} = \frac{16\pi\rho_{l0}^2 a_0^6 P_A^2}{p_0^2} \Omega^4 |A_{1P}(\Omega)|^4 \Gamma,$$
(102b)

with

$$\Gamma = \left| 1 + \frac{\phi_2^*(\Omega)}{\Omega_0^2 - 4\Omega^2 + S_{ac}(2\Omega) + S_{el}(2\Omega) + 4i\Omega\beta(2\Omega)} \right|^2.$$
(103)

Note that P_A is nondimensional.

The resonance frequency of bubble oscillation is usually evaluated from the curves for the scattering cross section at the driving frequency. It is taken to be equal to the frequency f_{max} at which σ_{s1} has a local maximum. However, the frequency f_{max} differs from the resonance frequency due to the
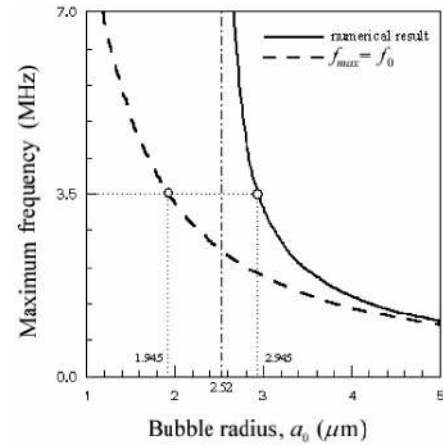

FIG. 9. Maximum frequency f_{max} (solid) for an encapsulated microbubble in an incompressible Newtonian liquid, as a function of bubble radius, compared with the undamped natural frequency f_0 (dashed). The same parameters as in Fig. 6.

presence of Ω^4 in the numerator of Eq. (102a). In the case of an incompressible Newtonian liquid, when thermal effects are neglected, it is easy to obtain that

$$f_{max} = f_{max1} = \frac{f_0^2}{f_{res}}.$$
(104)

If viscous damping is small (large bubbles), we can neglect the difference between f_{res} and f_0 and then f_{max} is approximately equal to the undamped natural frequency. This is not true for microbubbles with the radius less than 5 μm for which f_{res} greatly differs from f_0 (see above). From Eq. (104) and the existence of the critical bubble radius a_{0c} at which $f_{res} = 0$ it follows that the frequency f_{max} tends to infinity as the bubble radius approaches a_{0c}, though the undamped natural frequency goes to infinity at $a_0 = 0$. The result is practically unaffected if thermal effects are allowed for. Figure 9 shows the dependence of the maximum frequency f_{max} on the bubble radius a_0 for the encapsulated microbubble in an incompressible Newtonian liquid, as obtained from the numerical maximization of the scattering cross section σ_{s1}. The frequency goes to infinity at the point $a_0 = 2.52$ μm which is very close to the critical value for the resonance frequency (2.6 μm). Experimentalists define the resonance radius of the bubble from the resonant peaks in the scattering cross-section curves. However, it is difficult to construct the dependence of σ_{s1} on a_0 because of polydispersity of real microbubble suspensions. However, there is no problem to measure the scattered pressure field for a particular value of the driving frequency. Therefore, specialists in acoustic scattering make use of the plots of scattering cross section versus frequency for defining the maximum frequency f_{max} (which is considered as the resonance frequency). The resonance radius of the bubble can then be found from the $f_{max} - a_0$ curves.[75] Previously, the assumption $f_{max} = f_0$ was used for calculating the resonance bubble radius, i.e., the undamped natural frequency was considered to be the frequency at which the scattering cross section had a local maximum. As seen in Fig. 9, this assumption, which works only for large bubbles, leads to underestimating the
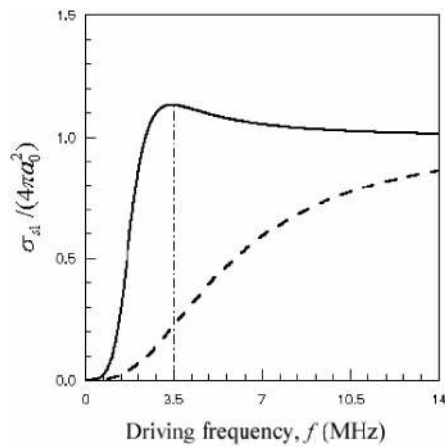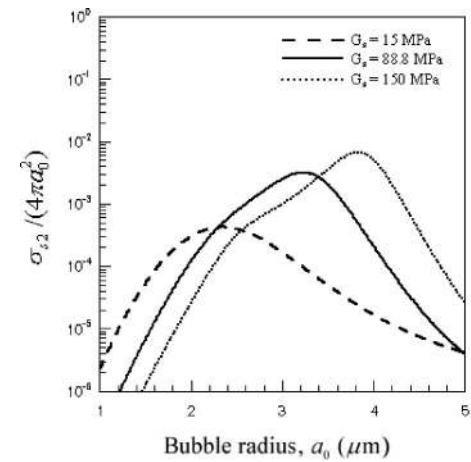
FIG. 10. First-harmonic scattering cross section versus driving frequency. The solid line is for $a_0 = 2.945$ μm, the dashed line for $a_0 = 1.945$ μm. The surrounding liquid is incompressible and Newtonian.

resonant size of microbubbles. For the parameters of this figure, the undamped natural frequency gives the resonant radius of 1.945 μm at the driving frequency $f = 3.5$ MHz. However, the actual resonant radius is 2.945 μm (Fig. 9). Indeed, for a microbubble with the radius of 2.945 μm the scattering cross section σ_{s1} has a maximum at the driving frequency of 3.5 MHz. However, there is no resonant peak in σ_{s1} at 3.5 MHz for a 1.945 μm bubble (Fig. 10). Moreover, the scattering cross section never reaches a local maximum for such a microbubble because its radius is below the critical value.

　　Figures 11 and 12 show the effects of the shell parameters (elasticity, viscosity, and thickness) and of the compressibility and viscoelasticity of the surrounding liquid on the second-harmonic scattering cross section σ_{s2}. First, an increase in the shell elasticity results in increasing the magnitude of the resonant peak in σ_{s2} [Fig. 11(a)]. This contradicts one of Church's conclusions that "the magnitude and the sharpness of the peaks in the cross section curves tend to decrease as the shell rigidity increases." [5] It is easy to check that the derivative of σ_{s1} or σ_{s2} with respect to G_s is always positive, i.e., the scattering cross sections increase with increasing shell elasticity. Of course, the scattering is weaker for microbubbles with more viscous shells [Fig. 11(b)]. Therefore, viscosity of the shell is the main reason why the encapsulated microbubbles scatter more poorly than free microbubbles. It should be noted that the second-harmonic resonance, which takes place if the driving frequency is equal to $f_{max}/2$, appears only for reasonably small values of the shell viscosity [see the dashed line in Fig. 11(b)]. As seen in Fig. 11(c), the microbubbles with thick shells are poor scatterers in comparison with those with thin shells. This is because an increase in the shell thickness leads to the increased impact of the shell viscosity on microbubble oscillations.
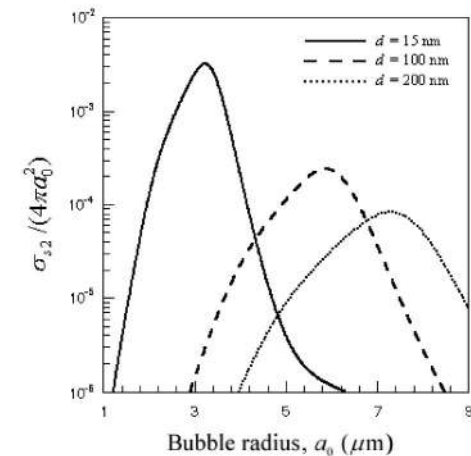
　　The liquid parameters weakly affect the scattering by the encapsulated microbubbles as compared to the shell parameters. The magnitude of the resonant peak in the scattering cross section curves tends to decrease with decreasing speed of sound in the liquid because of acoustic radiation

(a)
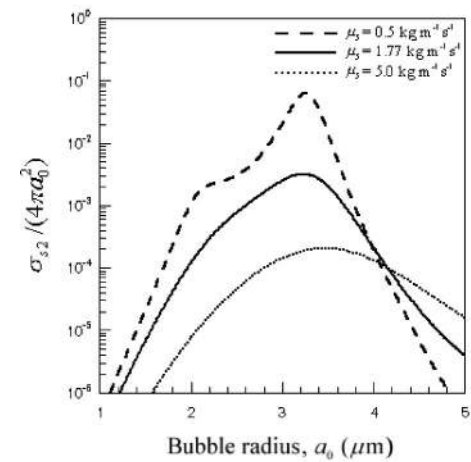
(b)

(c)

FIG. 11. Second-harmonic scattering cross section versus bubble radius for an encapsulated microbubble in a compressible Newtonian liquid for different values of (a) shell elasticity, (b) shell viscosity, and (c) shell thickness. $P_A = 0.3$, other parameters are given in Fig. 7.

damping [Fig. 12(a)]. The resonant scattering by the microbubbles is higher in a viscoelastic liquid than in a Newtonian liquid. The larger the relaxation time, the higher the resonant peak [Fig. 12(b)]. It is worth noting that the magnitude of the resonance peak at $C_l = \infty$ differs from that at
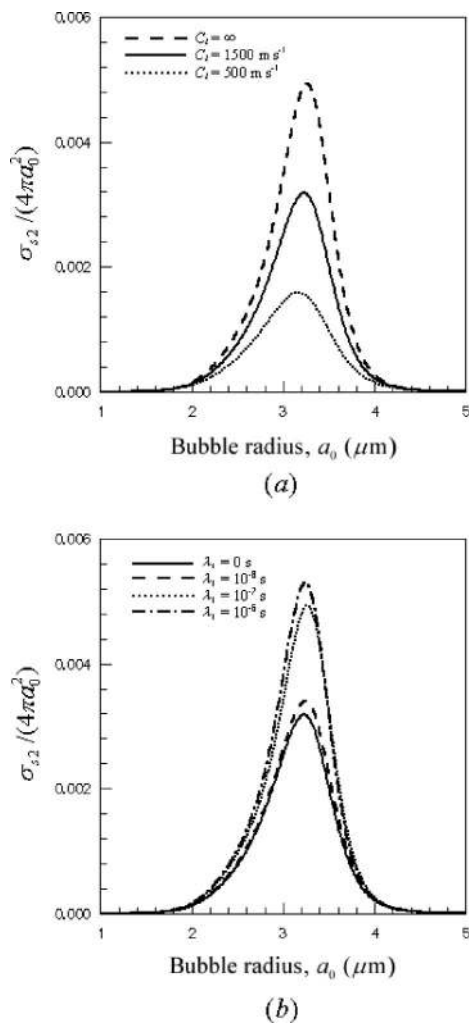
FIG. 12. Effects of (a) liquid compressibility and (b) viscoelasticity on the second-harmonic scattering cross section. The parameter $P_A = 0.3$. For plot (a) $\lambda_1 = \lambda_2 = 0$ s, for (b) $C_l = 1500$ m/s and $\lambda_2 = 0$ s.

$C_l = 1500$ m/s by a factor of about 1.5. The same difference is seen between a Newtonian liquid and a viscoelastic liquid with the relaxation time 10^{-6} s. Moreover, the relaxation time for blood may be higher. For example, the characteristic time for red cell deformation may reach 0.06 s (see Ref. 53). The effects of liquid compressibility and elasticity are therefore detectable by current experimental technique.[76]

VI. CONCLUSIONS

In this study, the equation for radial oscillations of an encapsulated gas bubble in a compressible viscoelastic liquid has been derived using the method of matched asymptotic expansions. The Kelvin–Voigt and 4-constant Oldroyd models were adopted to describe the viscoelastic properties of the encapsulating layer and of the liquid, respectively. Based on this equation, the small-amplitude forced oscillations of the encapsulated microbubble were analyzed. The formulas for the first- and second-harmonic amplitudes of bubble oscillation and the expressions for the scattering cross sections at the driving frequency and at twice that frequency were presented.

We have shown that if the bubble is small (~ 2 μm in size) and is covered by a shell 15 nm (or more) in thickness, the total damping of its radial oscillation is determined by the shell viscosity. In the viscoelastic liquid case, the contribution of the liquid viscosity to the total damping coefficient is below that for a Newtonian liquid and sharply decreases with frequency even at small values of the relaxation time. The numerical maximization of the amplitude-frequency response function reveals that the resonance frequency for the encapsulated bubble of radius $a_0 < 5$ μm highly depends on the shell and liquid viscosities, and therefore, significantly differs from the undamped natural frequency. Hence, the presently accepted assumption $f_{res} = f_0$ fails over a range of ultrasound contrast agents. Moreover, at given values for the shell and liquid parameters there exists a critical value of the bubble radius such that any smaller microbubble does not resonate. This critical radius is about 1.5 μm for the microbubble surrounded by blood and encapsulated by 15 nm thick shell having elasticity $G_s = 88.8$ MPa and viscosity $\mu_s = 1.77$ kg m^{-1} s^{-1}. Recall that these values correspond to those obtained by fitting the de Jong theory with experimental data for Albunex® bubbles (see Refs. 6 and 5).

Usually, experimentalists consider the frequency at which the first-harmonic scattering cross section is maximal as the resonance frequency of bubble oscillation. This is not true for micron bubbles. Upon neglecting thermal effects and considering the liquid to be Newtonian and incompressible, this maximum frequency f_{max} can be expressed in terms of the undamped natural and resonance frequencies as $f_{max} = f_0^2/f_{res}$. When the bubble radius approaches the critical value, this maximum frequency tends to infinity, whereas the resonance frequency tends to zero. Also, the assumption $f_{max} = f_0$, which is used for evaluating the resonance bubble size from the experimental data on the scattering cross section (vs the driving frequency), is no longer valid for the encapsulated microbubbles. In the range of medical ultrasound frequencies it leads to significant underestimation of the resonance bubble size.

The resonant peaks in the scattering cross section curves are very sensitive to the shell parameters but not to the liquid parameters. The effects of liquid compressibility and viscoelasticity on the scattering by the encapsulated microbubbles are, therefore, small. There is a slight increase in the magnitude of the peaks with decreasing the liquid viscosity or the speed of sound in the liquid and with increasing the relaxation time. But these effects are detectable based on the sensitivity of current experiments. The experimental results, which indicate that the encapsulated microbubbles scatter ultrasound more poorly than free ones, are due to the shell viscosity. It is not true that the shell elasticity is responsible for that. The scattering cross sections increase with increasing the shell elasticity. If the shell becomes thicker, the scattering deteriorates. This can also be explained by the increased impact of the shell viscosity on microbubble oscillations.

awarded in 2000. Any opinions, findings, conclusions or rec-ommendations expressed in this publication are those of the authors and do not necessarily reflect the view of NATO. The authors are indebted to Professor Ronald A. Roy and Professor R. Glynn Holt for helpful discussions.

APPENDIX: SMALL-AMPLITUDE ANALYSIS OF THE CONSTITUTIVE EQUATION

The effects of liquid compressibility are negligible near the bubble surface. In that case, the 4-constant Olrdroyd constitutive model is reduced to the system of equations [see Eqs. (36)]:

$$\left[1+\mathrm{De}\frac{\partial}{\partial t_*}+\frac{\mathrm{De}\,Q(t_*)}{r_*^2}\left(\frac{\partial}{\partial r_*}+\frac{2}{r_*}\right)\right]\tau_{*rr}^{(ld)}$$

$$=2\left(\eta-\frac{2}{3}\right)\frac{\mathrm{De}\,Q(t_*)}{r_*^3}\mathrm{tr}[\boldsymbol{\tau}_*^{(l)}]$$

$$-\frac{4}{\mathrm{Re}_l\,r_*^3}\left[Q(t_*)+\lambda\mathrm{De}\frac{dQ}{dt_*}-\lambda\mathrm{De}\frac{Q^2(t_*)}{r_*^3}\right], \quad (A1a)$$

$$\left[1+\mathrm{De}\frac{\partial}{\partial t_*}+\frac{\mathrm{De}\,Q(t_*)}{r_*^2}\frac{\partial}{\partial r_*}\right]\mathrm{tr}[\boldsymbol{\tau}_*^{(l)}]$$

$$=-\frac{6\mathrm{De}\,Q(t_*)}{r_*^3}\tau_{*rr}^{(ld)}-\frac{24\lambda\mathrm{De}\,Q^2(t_*)}{\mathrm{Re}_l\,r_*^6}, \quad (A1b)$$

where the function

$$Q(t_*)=a_*^2(t_*)\frac{da_*}{dt_*}. \quad (A2)$$

If the amplitude of the incident acoustic field is small, i.e., the bubble undergoes small-amplitude oscillations

$$a_*(t_*)=1+x_1(t_*),$$

$$x_1(t_*)=\varepsilon_p x_1(t_*)+\varepsilon_p^2 x_2(t_*)+O(\varepsilon_p^3), \quad (A3)$$

we can seek the solution of Eqs. (A1) as expansion in powers of a small parameter ε_p

$$\tau_{*rr}^{(ld)}=\varepsilon_p T_1+\varepsilon_p^2 T_2+O(\varepsilon_p^3), \quad \mathrm{tr}[\boldsymbol{\tau}_*^{(l)}]=\varepsilon_p Y_1+\varepsilon_p^2 Y_2+O(\varepsilon_p^3). \quad (A4)$$

To obtain the equations for stress perturbations we substitute (A3) and (A4) into the system (A1) and separate the resulting expressions in the orders of ε_p. The first-order equations look as follows:

$$\left(1+\mathrm{De}\frac{\partial}{\partial t_*}\right)T_1=-\frac{4}{\mathrm{Re}_l\,r_*^3}\left(1+\lambda\mathrm{De}\frac{\partial}{\partial t_*}\right)\frac{dx_1}{dt_*}, \quad Y_1=0. \quad (A5)$$

From the second equation of (A5) it follows that the trace of the shear stress tensor $\mathrm{tr}[\boldsymbol{\tau}_*^{(l)}]$ is a quadratic nonlinear term (of order ε_p^2). The second-order equations then have the form

$$\left(1+\mathrm{De}\frac{\partial}{\partial t_*}\right)T_2$$

$$=-\frac{\mathrm{De}}{r_*^2}\frac{dx_1}{dt_*}\left(\frac{\partial}{\partial r_*}+\frac{2}{r_*}\right)T_1-\frac{4}{\mathrm{Re}_l\,r_*^3}\left(1+\lambda\mathrm{De}\frac{\partial}{\partial t_*}\right)$$

$$\times\left(\frac{dx_2}{dt_*}+2x_1\frac{dx_1}{dt_*}\right)+\frac{4\lambda\mathrm{De}}{\mathrm{Re}_l\,r_*^6}\left(\frac{dx_1}{dt_*}\right)^2, \quad (A6a)$$

$$\left(1+\mathrm{De}\frac{\partial}{\partial t_*}\right)Y_2=-\frac{6\mathrm{De}}{r_*^3}\frac{dx_1}{dt_*}T_1-\frac{24\lambda\mathrm{De}}{\mathrm{Re}_l\,r_*^6}\left(\frac{dx_1}{dt_*}\right)^2. \quad (A6b)$$

These equations are uncoupled because the only interaction term in Eq. (A1a)

$$2\left(\eta-\frac{2}{3}\right)\frac{\mathrm{De}\,Q(t_*)}{r_*^3}\mathrm{tr}[\boldsymbol{\tau}_*^{(l)}],$$

is of order ε_p^3. Therefore, this term should be taken into account only in the equations for the third- and higher-order stress perturbations. This means that the trace of the shear stress tensor affects neither the first harmonic nor the second harmonic of bubble oscillation. Indeed, the integral

$$q(t_*)=3\int_{R_*(t_*)}^{\infty}\frac{\tau_{*\widetilde{r}\widetilde{r}}^{(ld)}}{\widetilde{r}}d\widetilde{r},$$

the contribution of liquid viscoelasticity to bubble oscillations, does not depend on the third-order stress perturbation T_3 if we restrict our attention to the quadratic nonlinear terms. This is because r_* is of order of unity and the integral is not singular at any value of t_*, at least, in the case of small-amplitude oscillations. Using Eqs. (A3) and (A4), we can write this integral in the form

$$q(t_*)=3\int_{R_*(t_*)}^{\infty}\frac{\varepsilon_p T_1+\varepsilon_p T_2}{\widetilde{r}}d\widetilde{r}+O(\varepsilon_p^3),$$

$$R_*(t_*)=\frac{R_0}{a_0}\left[1+\varepsilon_p\frac{a_0^3}{R_0^3}x_1(t_*)+O(\varepsilon_p^2)\right]. \quad (A7)$$

The first- and second-order stress perturbations T_1 and T_2, which are the solutions of the first equation of (A5) and Eq. (A6a), can be represented as

$$T_1=\frac{h_1(t_*)}{r_*^3}, \quad T_2=\frac{h_2(t_*)}{r_*^3}+\frac{g_2(t_*)}{r_*^6}, \quad (A8)$$

where the functions $h_1(t_*)$, $h_2(t_*)$, and $g_2(t_*)$ are solutions of the following ordinary differential equations:

$$\left(1+\mathrm{De}\frac{d}{dt}\right)h_1(t_*)=-\frac{4}{\mathrm{Re}_l}\left(1+\lambda\mathrm{De}\frac{d}{dt}\right)\frac{dx_1}{dt_*}, \quad (A9)$$

$$\left(1+\mathrm{De}\frac{d}{dt}\right)h_2(t_*)=-\frac{4}{\mathrm{Re}_l}\left(1+\lambda\mathrm{De}\frac{d}{dt}\right)$$

$$\times\left(\frac{dx_2}{dt_*}+2x_1\frac{dx_1}{dt_*}\right), \quad (A10)$$

$$\left(1+\mathrm{De}\frac{d}{dt}\right)g_2(t_*)=\mathrm{De}\frac{dx_1}{dt_*}h_1(t_*)+\frac{4\lambda\mathrm{De}}{\mathrm{Re}_l}\left(\frac{dx_1}{dt_*}\right)^2. \quad (A11)$$

Substitution of (A8) into (A7) and further integration of the result yield

$$q(t_*) = \varepsilon_p \frac{a_0^3}{R_0^3} h_1(t_*) + \varepsilon_p^2 \left[-\frac{3a_0^6}{R_0^6} h_1(t_*) x_1(t_*) \right.$$
$$\left. + \frac{a_0^3}{R_0^3} h_2(t_*) + \frac{a_0^6}{2R_0^6} g_2(t_*) \right] + O(\varepsilon_p^3). \qquad (A12)$$

Expression (A12) takes the form of Eq. (60) after some rearrangement and reverting to the variable $x(t_*)$.

[1] F. Calliada, R. Campani, O. Bottinelli, A. Bozzini, and M. G. Sommaruga, "Ultrasound contrast agents. Basic principles," Eur. J. Radiol. **27**, S157 (1998).

[2] P. J. A. Frinking, A. Bouakaz, J. Kirkhorn, F. J. Ten Cate, and N. de Jong, "Ultrasound contrast imaging: current and new potential methods," Ultrasound Med. Biol. **26**, 965 (2000).

[3] P. N. T. Wells, "Ultrasonic imaging of the human body," Rep. Prog. Phys. **62**, 671 (1999).

[4] N. de Jong, "Acoustic properties of ultrasound contrast agents," Ph.D. thesis, Erasmus University, Rotterdam, The Netherlands (1993).

[5] C. C. Church, "The effects of an elastic solid surface layer on the radial pulsations of gas bubbles," J. Acoust. Soc. Am. **97**, 1510 (1995).

[6] N. de Jong and L. Hoff, "Ultrasound scattering of Albunex® microspheres," Ultrasonics **31**, 175 (1993).

[7] P. J. A. Frinking and N. de Jong, "Acoustic modeling of shell-encapsulated gas bubbles," Ultrasound Med. Biol. **24**, 523 (1998).

[8] L. Hoff, P. C. Sontum, and J. M. Hovem, "Oscillations of polymeric microbubbles: Effect of the encapsulating shell," J. Acoust. Soc. Am. **107**, 2272 (2000).

[9] Y. C. Fung, *Biomechanics: Mechanical Properties of Living Tissue* (Springer-Verlag, New York, 1993).

[10] Y. C. Fung, *Biomechanics: Circulation* (Springer-Verlag, New York, 1996).

[11] B. A. J. Angelsen, *Ultrasound Imaging—Waves, Signals, and Signal Processing, Vols. 1 and 2* (Emantec, Trondheim, 2000).

[12] G. B. Thurston, "Viscoelastic properties of blood and blood analogs" in *Advances in Hemodynamics and Hemorheology*, edited by T. V. How (JAI, Greenwich, 1996), pp. 1–30.

[13] C. T. Chin and P. N. Burns, "Predicting the acoustic response of a microbubble population for contrast imaging in medical ultrasound," Ultrasound Med. Biol. **26**, 1293 (2000).

[14] N. G. Page, A. Cowley, and A. M. Campbell, "Short pulse acoustic excitation of microbubbles," J. Acoust. Soc. Am. **102**, 1474 (1997).

[15] D. L. Miller, "Frequency relationships for ultrasonic activation of free microbubbles, encapsulated microbubbles, and gas-filled micropores," J. Acoust. Soc. Am. **104**, 2498 (1998).

[16] W. Lauterborn, "Numerical investigation of nonlinear oscillations of gas bubbles in liquids," J. Acoust. Soc. Am. **59**, 283 (1976).

[17] L. A. Crum and A. Prosperetti, "Nonlinear oscillations of gas bubbles in liquids: An interpretation of some experimental results," J. Acoust. Soc. Am. **73**, 121 (1982).

[18] P. N. Burns, D. H. Simpson, and M. A. Averkiou, "Nonlinear imaging," Ultrasound Med. Biol. **26**, S19 (2000).

[19] P. J. A. Frinking, A. Bouakaz, N. de Jong, F. J. Ten Cate, and S. Keating, "Effect of ultrasound on the release of micro-encapsulated drugs," Ultrasonics **36**, 709 (1998).

[20] M. W. Miller, "Gene transfection and drug delivery," Ultrasound Med. Biol. **26**, S59 (2000).

[21] A. L. Klibanov, "Targeted delivery of gas-filled microspheres, contrast agents for ultrasound imaging," Adv. Drug Delivery Rev. **37**, 139 (1999).

[22] E. C. Unger, T. A. Fritz, T. Matsunaga, V. R. Ramaswami, D. Yellowhair, and G. Wu, "Therapeutic drug delivery systems," US Patent No. 5770222 (1998).

[23] P. A. Dayton, K. E. Morgan, A. L. Klibanov, G. H. Brandenburger, and K. W. Ferrara, "Optical and acoustical observations of the effects of ultrasound on contrast agents," IEEE Trans. Ultrason. Ferroelectr. Freq. Control **46**, 220 (1999).

[24] P. Jauregi and J. Varley, "Colloidal gas aphrons: potential applications in biotechnology," Trends Biotechnol. **17**, 389 (1999).

[25] R. I. Nigmatulin, *Dynamics of Multiphase Media, Vol. 1* (Hemisphere, Washington, 1990).

[26] M. S. Plesset and A. Prosperetti, "Bubble dynamics and cavitation," Annu. Rev. Fluid Mech. **9**, 145 (1977).

[27] I. Sh. Akhatov, N. K. Vakhitova, G. Ya. Galeyeva, R. I. Nigmatulin, and D. B. Khismatullin, "Weak oscillations of a gas bubble in a spherical volume of compressible liquid," J. Appl. Math. Mech. **61**, 921 (1997).

[28] A. Prosperetti, "Thermal effects and damping mechanisms in the forced radial oscillations of gas bubbles in liquids," J. Acoust. Soc. Am. **61**, 17 (1977).

[29] A. Prosperetti, "The thermal behavior of oscillating gas bubbles," J. Fluid Mech. **222**, 587 (1991).

[30] R. B. Chapman and M. S. Plesset, "Thermal effects in the free oscillation of gas bubbles," J. Basic Eng. **93**, 373 (1971).

[31] I. M. Ward, *Mechanical Properties of Solid Polymers* (Wiley, Chichester, 1983).

[32] E. A. Evans and R. M. Hochmuth, "Membrane viscoelasticity," Biophys. J. **16**, 1 (1976).

[33] L. D. Landau and E. M. Lifshitz, *Fluid Mechanics* (Pergamon, Oxford, 1987).

[34] C. Pozrikidis, *Introduction to Theoretical and Computational Fluid Dynamics* (Oxford University Press, New York, 1997).

[35] R. B. Bird, R. C. Armstrong, and O. Hassager, *Dynamics of Polymeric Liquids, Vol. 1: Fluid Mechanics* (Wiley, New York, 1987).

[36] P. J. Oliveira, "A traceless stress tensor formulation for viscoelastic fluid flow," J. Non-Newtonian Fluid Mech. **95**, 55 (2000).

[37] A. Prosperetti and A. Lezzi, "Bubble dynamics in a compressible liquid. Part 1. First-order theory," J. Fluid Mech. **168**, 457 (1986).

[38] A. Lezzi and A. Prosperetti, "Bubble dynamics in a compressible liquid. Part 2. Second-order theory," J. Fluid Mech. **185**, 289 (1987).

[39] E. A. Brujan, "A first-order model for bubble dynamics in a compressible viscoelastic liquid," J. Non-Newtonian Fluid Mech. **84**, 83 (1999).

[40] D. N. Ku, "Blood flow in arteries," Annu. Rev. Fluid Mech. **29**, 399 (1997).

[41] T. G. Pedley, *The Fluid Mechanics of Large Blood Vessels* (Cambridge University Press, Cambridge, 1980).

[42] G. Gormley and J. Wu, "Observation of acoustic streaming near Albunex® spheres," J. Acoust. Soc. Am. **104**, 3115 (1998).

[43] W. C. Moss, D. B. Clarke, J. W. White, and D. A. Young, "Hydrodynamic simulations of bubble collapse and picosecond sonoluminecence," Phys. Fluids **6**, 2979 (1994).

[44] W. C. Moss, "Understanding the periodic driving pressure in the Rayleigh–Plesset equation," J. Acoust. Soc. Am. **101**, 1187 (1997).

[45] R. I. Nigmatulin, I. Sh. Akhatov, N. K. Vakhitova, and R. T. Lahey, Jr., "On the forced oscillations of a small gas bubble in a spherical liquid-filled flask," J. Fluid Mech. **414**, 47 (2000).

[46] J. S. Allen and R. A. Roy, "Dynamics of gas bubbles in viscoelastic fluids. II. Nonlinear viscoelasticity," J. Acoust. Soc. Am. **108**, 1640 (2000).

[47] J. B. Keller and M. Miksis, "Bubble oscillations of large amplitude," J. Acoust. Soc. Am. **68**, 628 (1980).

[48] D. Cosgrove, "Echo enhancers and ultrasound imaging," Eur. J. Radiol. **26**, 64 (1997).

[49] T. G. Leighton, *The Acoustic Bubble* (Academic, London, 1994).

[50] C. Christiansen, H. Kryvi, P. C. Sontum, and T. Skotland, "Physical and biochemical characterization of Albunex, a new ultrasound contrast agent consisting of air-filled albumin microspheres suspended in a solution of human albumin," Biotechnol. Appl. Biochem. **19**, 307 (1994).

[51] J. N. Marsh, C. S. Hall, M. S. Hughes, J. Mobley, J. G. Miller, and G. H. Brandenburger, "Broadband through-transmission signal loss measurements of Albunex suspensions at concentrations approaching *in vivo* doses," J. Acoust. Soc. Am. **101**, 1155 (1997).

[52] S. Chien, "Shear dependence of effective cell volume as a determinant of blood viscosity," Science **168**, 977 (1970).

[53] G. R. Cokelet, "The rheology and tube flow of blood," in *Handbook of Bioengineering*, edited by R. Skalak and S. Chien (McGraw-Hill, New York, 1986), pp. 14.1–14.17.

[54] C. M. Rodkiewicz, P. Sinha, and J. S. Kennedy, "On the application of a constitutive equation for whole blood," J. Biomech. Eng. **112**, 198 (1990).

[55] W. W. Nichols and M. F. O'Rourke, *McDonald's Blood Flow in Arteries* (Lea & Febiger, Philadelphia, 1990).

[56] D. A. McDonald, *Blood Flow in Arteries* (Edward Arnold, London, 1974).

[57] H. Schmid-Schönbein, "The clinical significance of hemorheology," in *The Rheology of Blood, Blood Vessels and Associated Tissues*, edited by

D. R. Gross and N. H. C. Hwang (Sijthoff & Noordhoff, Alphen aan den Rijn, 1981), pp. 1–21.

[58] D. E. Brooks, T. W. Goodwin, and G. V. F. Seaman, "Interactions among erythrocytes under shear," J. Appl. Physiol. **28**, 172 (1970).

[59] S. Goto, N. Tamura, M. Sakakibara, Y. Ikeda, and S. Handa, "Effects of ticlopidine on von Willebrand factor-mediated shear-induced platelet activation and aggregation," Platelets **12**, 406 (2001).

[60] G. B. Thurston, "Erythrocyte rigidity as a factor in blood rheology: Viscoelastic dilatancy," J. Rheol. **23**, 703 (1979).

[61] G. B. Thurston, "Significance and methods of measurement of viscoelastic behavior of blood," in *The Rheology of Blood, Blood Vessels and Associated Tissues*, edited by D. R. Gross and N. H. C. Hwang (Sijthoff & Noordhoff, Alphen aan den Rijn, 1981), pp. 236–256.

[62] D. Schneditz, F. Rainer, and T. Kenner, "Viscoelastic properties of whole blood: Influence of fast sedimenting red blood cell aggregates," Biorheology **24**, 13 (1987).

[63] A. Kulmyrzaev and D. J. McClements, "High frequency dynamic shear rheology of honey," J. Food. Eng. **45**, 219 (2000).

[64] W. M. Phillips and S. Deutsch, "Toward a constitutive equation for blood," Biorheology **12**, 383 (1975).

[65] H. Chmiel and E. Walitza, *On the Rheology of Blood and Synovial Fluids* (Research Studies, New York, 1980).

[66] S. Deutsch and W. M. Phillips, "The use of the Taylor–Couette stability problem to validate a constitutive equation for blood," Biorheology **14**, 253 (1977).

[67] G. Pontrelli, "Pulsatile blood flow in a pipe," Comput. Fluids **27**, 367 (1998).

[68] A. Leuprecht and K. Perktold, "Computer simulation of non-newtonian effects on blood flow in large arteries," Comput. Methods Biomech. Biomed. Engin. **4**, 149 (2001).

[69] J. Lubbers, K. Ramnarine, and P. R. Hoskins, "Blood mimicking fluid for flow Doppler test object," Eur. J. Ultrasound **7**, S16 (1998).

[70] C. J. P. M. Teirlinck, R. A. Bezemer, C. Kollmann, J. Lubbers, P. R. Hoskins, P. Fish, K.-E. Fredfeldt, and U. G. Schaarschmidt, "Development of an example flow test object and comparison of five of these test objects, constructed in various laboratories," Ultrasonics **36**, 653 (1998).

[71] V. Sboros, C. M. Moran, T. Anderson, S. D. Pye, I. C. Macleod, A. M. Millar, and W. N. McDicken, "Evaluation of an experimental system for the *in vitro* assessment of ultrasonic contrast agents," Ultrasound Med. Biol. **26**, 105 (2000).

[72] G. R. Cokelet, "Rheology and hemodynamics," Annu. Rev. Physiol. **42**, 311 (1980).

[73] V. N. Alekseev and S. A. Rybak, "The behavior of gas bubbles in insonated biological tissues," Acoust. Phys. **44**, 243 (1998).

[74] J. S. Allen and R. A. Roy, "Dynamics of gas bubbles in viscoelastic fluids. I. Linear viscoelasticity," J. Acoust. Soc. Am. **107**, 3167 (2000).

[75] V. L. Newhouse and P. M. Shankar, "Bubble size measurements using the nonlinear mixing of two frequencies," J. Acoust. Soc. Am. **75**, 1473 (1984).

[76] R. A. Roy and R. E. Apfel, "Mechanical characterization of microparticles by scattered ultrasound," J. Acoust. Soc. Am. **87**, 2332 (1990).